

We are IntechOpen, the world's leading publisher of Open Access books Built by scientists, for scientists

6,900

Open access books available

186,000

International authors and editors

200M

Downloads

Our authors are among the

154

Countries delivered to

TOP 1%

most cited scientists

12.2%

Contributors from top 500 universities



WEB OF SCIENCE™

Selection of our books indexed in the Book Citation Index
in Web of Science™ Core Collection (BKCI)

Interested in publishing with us?
Contact book.department@intechopen.com

Numbers displayed above are based on latest data collected.
For more information visit www.intechopen.com



Quantitative Feedback Theory and Its Application in UAV's Flight Control

Xiaojun Xing and Dongli Yuan
Northwestern Polytechnical University, Xi'an,
China

1. Introduction

Quantitative feedback theory (hereafter referred as QFT), developed by Isaac Horowitz (Horowitz, 1963; Horowitz and Sidi, 1972), is a frequency domain technique utilizing the Nichols chart in order to achieve a desired robust design over a specified region of plant uncertainty. Desired time-domain responses are transformed into frequency domain tolerances, which lead to bounds (or constraints) on the loop transmission function. The design process is highly transparent, allowing a designer to see what trade-offs are necessary to achieve a desired performance level.

QFT is also a unified theory that emphasizes the use of feedback for achieving the desired system performance tolerances despite plant uncertainty and plant disturbances. QFT quantitatively formulates these two factors in the form of (a) the set $\mathfrak{S}_R = \{T_R\}$ of acceptable command or tracking input-output relationships and the set $\mathfrak{S}_D = \{T_D\}$ of acceptable disturbance input-output relationships, and (b) a set $\varphi = \{P\}$ of possible plants which include the uncertainties. The objective is to guarantee that the control ratio $T_R = Y / R$ is a member of \mathfrak{S}_R and $T_D = Y / D$ is a member of \mathfrak{S}_D , for all plants P which are contained in φ . QFT has been developed for control systems which are both linear and nonlinear, time-invariant and time-varying, continuous and sampled-data, uncertain multiple-input single-output (MISO) and multiple-input multiple-output (MIMO) plants, and for both output and internal variable feedback.

The QFT synthesis technique for highly uncertain linear time-invariant MIMO plants has the following features:

1. The MIMO synthesis problem is converted into a number of single-loop feedback problems in which parameter uncertainty, external disturbances, and performance tolerances are derived from the original MIMO problem. The solutions to these single-loop problems represent a solution to the MIMO plant.
2. The design is tuned to the extent of the uncertainty and the performance tolerances.

This design technique is applicable to the following problem classes:

1. Single-input single-output (SISO) linear-time-invariant (LTI) systems
2. SISO nonlinear systems.
3. MIMO LTI systems.
4. MIMO nonlinear systems.

5. Distributed systems.
6. Sampled-data systems as well as continuous systems for all of the preceding.

Problem classes 3 and 4 are converted into equivalent sets of MISO systems to which the QFT design technique is applied. The objective is to solve the MISO problems, i.e., to find compensation functions which guarantee that the performance tolerances for each MISO problem are satisfied for all P in φ .

This chapter is essentially divided into two parts. The first part, consisting of Sections 2 through 4, presents the fundamentals of the QFT robust control system design technique for the tracking and regulator control problems. The second part consists of Section 5 which focuses on the application of QFT technique to the flight control design for a certain Unmanned Aerial Vehicle (UAV). This is accomplished by decomposing the UAV's MIMO plant to 2 MISO plants whose controllers are both synthesized using QFT technique for MISO systems. And the effectiveness of both controllers is verified according to the digital simulation results. Besides, Sections 6 through 8 are about summary of whole chapter, references and symbols used in the chapter.

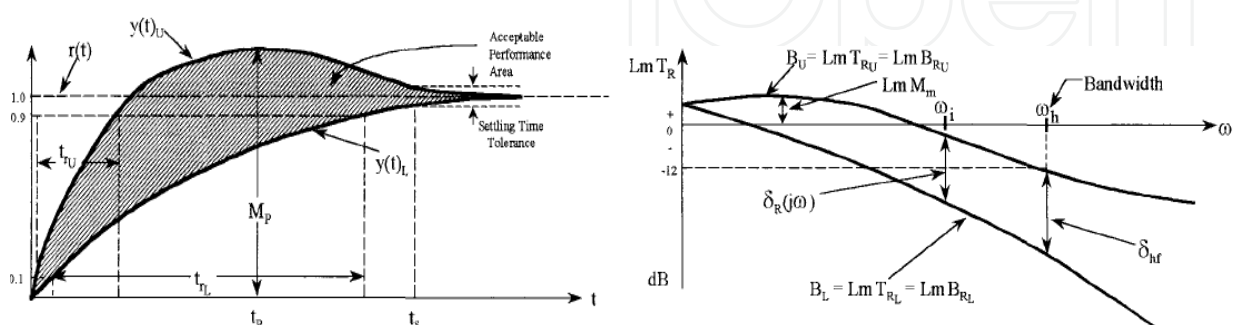
2. Overview of QFT

2.1 Design objective of QFT

Objective of QFT is to design and implement robust control for a system with structured parametric uncertainty that satisfies the desired performance specifications.

2.2 Performance specifications for control system

In many control systems the output $y(t)$ must lie between specified upper and lower bounds, $y(t)_U$ and $y(t)_L$, respectively, as shown in Fig.1a. The conventional time-domain figures of merit, based upon a step input signal $r(t)$ are shown in Fig.1a. They are: M_p , peak overshoot; t_r , rise time; t_p , peak time; and t_s , settling time. Corresponding system performance specifications in the frequency domain are, B_U and B_L , the upper and lower bounds respectively, peak overshoot $Lm M_m$, and the frequency bandwidth ω_h which are shown in Fig.1b.



(a) time domain response specifications (b) frequency domain response specifications

Fig. 1. Desired system performance specifications

Assume that the control system has negligible sensor noise and sufficient control effort authority, then for a stable LTI minimum-phase plant, a LTI compensator may be designed to achieve the desired control system performance specifications.

2.3 Implementation of QFT design objective

The QFT design objective is achieved by:

- Representing the characteristics of the plant and the desired system performance specifications in the frequency domain.
- Using these representations to design a compensator (controller).
- Representing the nonlinear plant characteristics by a set of LTI transfer functions that cover the range of structured parametric uncertainty.
- Representing the system performance specifications (see Fig.1) by LTI transfer functions that form the upper B_u and lower B_l boundaries for the design.
- Reducing the effect of parameter uncertainty by shaping the open-loop frequency responses so that the Bode plots of the J closed-loop systems fall between the boundaries B_u and B_l , while simultaneously satisfying all performance specifications.
- Obtaining the stability, tracking, disturbance, and cross-coupling (for MIMO systems) boundaries on the Nichols chart in order to satisfy the performance specifications.

2.4 QFT basics

Consider the control system of Fig.2, where $G(s)$ is a compensator, $F(s)$ is a prefilter, and φ is the nonlinear plant with structured parametric uncertainty. To carry out a QFT design:

- The nonlinear plant is described by a set of J minimum-phase LTI plants, i.e., $\varphi = \{P_t(s)\}(t = 1, 2, \dots, J)$ which define the structured plant parameter uncertainty.
- The magnitude variation due to the plant parameter uncertainty, $\delta_p(j\omega_i)$, is depicted by the Bode plots of the LTI plants as shown in Fig. 3 which is for a certain plant.
- J data points (log magnitude and phase angle), for each value of frequency, $\omega = \omega_i$, are plotted on the Nichols chart. A contour is drawn through the data points that described the boundary of the region that contains all J points. This contour is referred to as a template. It represents the region of structured plant parametric uncertainty on the Nichols chart and are obtained for specified values of frequency, $\omega = \omega_i$, within the bandwidth (BW) of concern. Six data points (log magnitude and phase angle) for each value of ω_i are obtained, as shown in Fig. 4a, for a certain example to plot the templates, for each value of ω_i , as shown in Fig. 4b.
- The system performance specifications are represented by LTI transfer functions, and their corresponding Bode plots are shown in Fig. 3 by the upper and lower bounds B_u and B_l , respectively.

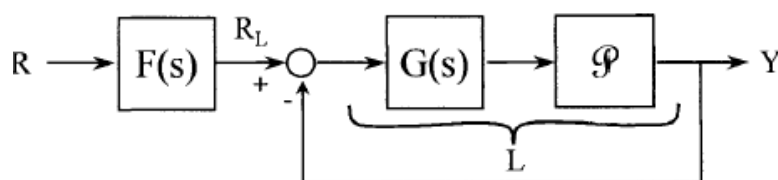


Fig. 2. Compensated nonlinear system

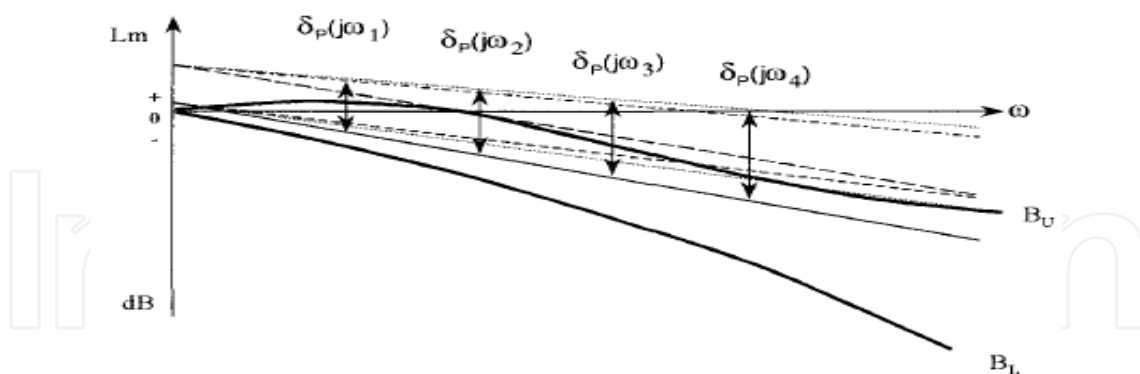
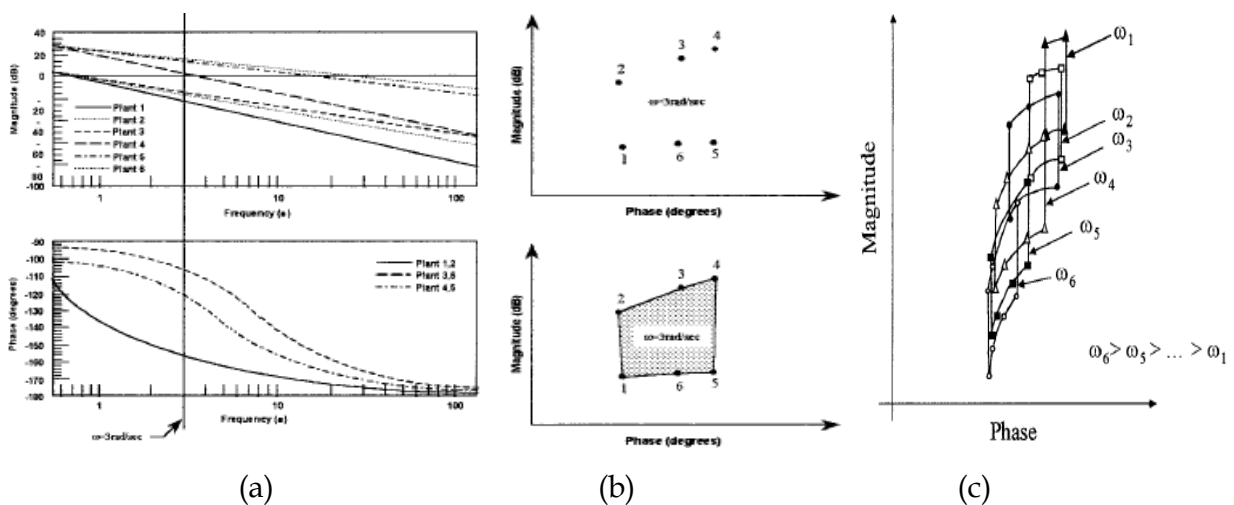


Fig. 3. LTI plants

Fig. 4. (a) Bode plots of 6 LTI plants; (b) template construction for $\omega = 3$ rad/sec; (c) construction of the Nichols chart plant templates

2.5 QFT design

The tracking design objective is to

- a. Synthesize a compensator $G(s)$ of Fig. 2 that
 - results in satisfying the desired performance specifications of Fig. 1
 - results in the closed-loop frequency responses T_{Li} shown in Fig. 5
 - results in the $\delta_L(j\omega_i)$ of Fig. 5 of the compensated system, being equal to or smaller than $\delta_P(j\omega_i)$ of Fig. 3 for the uncompensated system and that it is equal or less than $\delta_R(j\omega_i)$, for each value of ω_i of interest; that is: $\delta_L(j\omega_i) \leq \delta_R(j\omega_i) \leq \delta_P(j\omega_i)$
- b. Synthesize a prefilter $F(s)$ of Fig. 2 that results in shifting and reshaping the T_{Li} responses in order that they lie within the B_U and B_L boundaries in Fig. 5 as shown in Fig. 6.

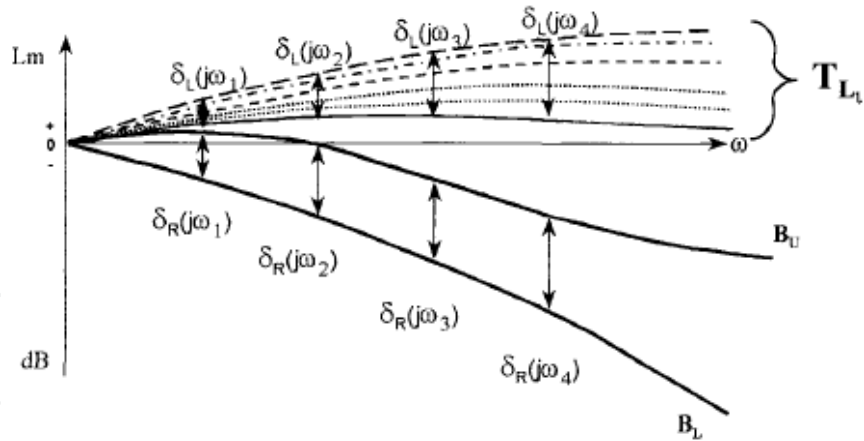


Fig. 5. Closed-loop responses: LTI plants with $G(s)$

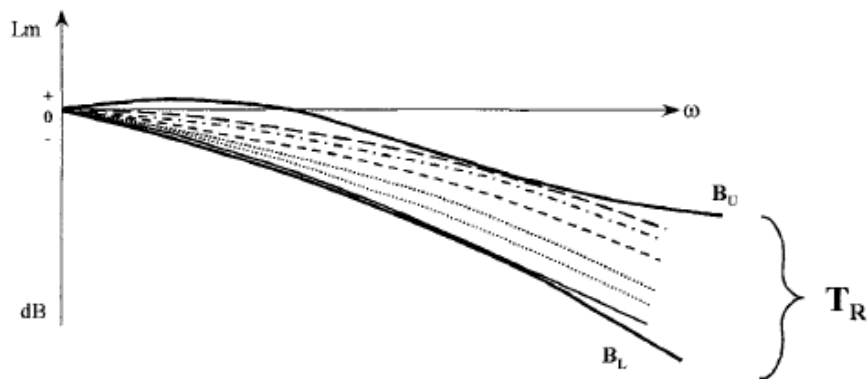


Fig. 6. Closed-loop responses: LTI plants with $G(s)$ and $F(s)$

Therefore, the QFT robust design technique assures that the desired performance specifications are satisfied over the prescribed region of structured plant parametric uncertainty.

3. Insight to the QFT technique

3.1 Open-loop plant

Consider a certain position control system whose plant transfer function is given by

$$P_i(s) = \frac{K_a}{s(s+a)} = \frac{K'}{s(s+a)} \tag{1}$$

where $K' = K_a$ and $i = 1, 2, \dots, J$. The log magnitude changes in a prescribed range due to the plant parameter uncertainty. The loop transmission $L(s)$ is defined as

$$L_i(s) = G(s)P_i(s) \tag{2}$$

3.2 Closed-loop formulation

The control ratio T_L of the unity-feedback system of Fig. 2 is

$$T_{Lt} = \frac{Y}{R_L} = \frac{L_t}{1 + L_t} \quad (3)$$

The overall system control ratio T_R

is given by:

$$T_{Rt}(s) = \frac{F(s)L_t(s)}{1 + L_t(s)} \quad (4)$$

3.3 Results of applying the QFT design technique

The proper application of the robust QFT design technique requires the utilization of the prescribed performance specifications from the onset of the design process, and the selection of a nominal plant P_o from the J LTI plants. Once the proper loop shaping of $L_o(s) = G(s)P_o(s)$ is accomplished, a synthesized $G(s)$ is achieved that satisfies the desired performance specifications. The last step of this design process is the synthesis of the prefilter that ensures that the Bode plots of T_{Ri} all lie between the upper and lower bounds B_U and B_L .

3.4 Benefits of QFT

The benefits of the QFT technique may be summarized as follows:

- It results in a robust design which is insensitive to structured plant parameter variation.
- There can be one robust design for the full, operating envelope.
- Design limitations are apparent up front and during the design process.
- The achievable performance specifications can be determined in the early design stage.
- If necessary, one can redesign for changes in the specifications quickly with the aid of the QFT CAD package.
- The structure of the compensator (controller) is determined up front.
- There is less development time for a full envelope design.

4. QFT design for the MISO analog control system

4.1 Introduction

The MIMO synthesis problem is converted into a number of single-loop feedback problems in which parameter uncertainty, cross-coupling effects, and system performance tolerances are derived from the original MIMO problem. The solutions to these single-loop problems represent a solution to the MIMO plant. It is not necessary to consider the complete system characteristic equation. The design is tuned to the extent of the uncertainty and the performance tolerances.

Here, we will present an in-depth understanding and appreciation of the power of the QFT technique through apply QFT to a robust single-loop MISO system, which has two inputs, a tracking and an external disturbance input, respectively, and a single output control system.

4.2 The QFT method (single-loop MISO system)

Basic structure of a feedback control system is given in Fig.7 , in which φ represents the set of transfer functions which describe the region of plant parameter uncertainty, G is the cascade compensator, and F is an input prefilter transfer function. The output $y(t)$ is required to track the command input $r(t)$ and to reject the external disturbances $d_1(t)$ and $d_2(t)$. The compensator G in Fig. 7 is to be designed so that the variation of $y(t)$ to the uncertainty in the plant P is within allowable tolerances and the effects of the disturbances $d_1(t)$ and $d_2(t)$ on $y(t)$ are acceptably small. Also, the prefilter properties of $F(s)$ must be designed to the desired tracking by the output $y(t)$ of the input $r(t)$. Since the control system in Fig. 7 has two measurable quantities, $r(t)$ and $y(t)$, it is referred to as a two degree-of-freedom (DOF) feedback structure. If the two disturbance inputs are measurable, then it represents a four DOF structure. The actual design is closely related to the extent of the uncertainty and to the narrowness of the performance tolerances. The uncertainty of the plant transfer function is denoted by the set

$$\varphi = \{P_t\} \quad \text{where } t = 1, 2, \dots, J \quad (5)$$

and is illustrated as follows.

Given that the plant transfer function is

$$P(s) = \frac{K}{s(s+a)} \quad (6)$$

where the value of K is in the range $[1, 10]$ and a is in the range $[-2, 2]$. The design objective is to guarantee that $T_r(s) = Y(s)/R(s)$ and $T_d(s) = Y(s)/D(s)$ are members of the sets of acceptable \mathfrak{S}_R and \mathfrak{S}_D for changes of K and a . In a feedback control system, the principal challenge in the control system design is to relate the system performance specifications to the requirements on the loop transmission function $L(s) = G(s)P(s)$ in order to achieve the desired benefits of feedback, i.e., the desired reduction in sensitivity to plant uncertainty and desired disturbance attenuation. The advantage of the frequency domain is that $L(s) = G(s)P(s)$ is simply the multiplication of complex numbers. In the frequency domain it is possible to evaluate $L(j\omega)$ at every ω_i separately, and thus, at each ω_i , the optimal bounds on $L(j\omega)$ can be determined.

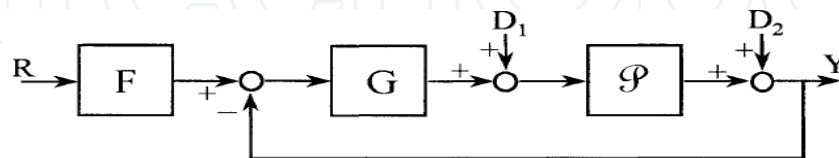


Fig. 7. A feedback structure

4.3 QFT design procedure

The objective is to design the prefilter $F(s)$ and the compensator $G(s)$ of Fig.7 so that the specified robust design is achieved for the given region of plant parameter uncertainty. The design procedure to accomplish this objective is as follows:

- Step 1.** Synthesize the desired tracking model.
- Step 2.** Synthesize the desired disturbance model.
- Step 3.** Specify the J LTI plant models that define the boundary of the region of plant parameter uncertainty.
- Step 4.** Obtain plant templates at specified frequencies that pictorially describe the region of plant parameter uncertainty on the Nichols chart.
- Step 5.** Select the nominal plant transfer function $P_o(s)$.
- Step 6.** Determine the stability contour (U -contour) on the Nichols chart.
- Step 7-9.** Determine the disturbance, tracking, and optimal bounds on the Nichols chart.
- Step 10.** Synthesize the nominal loop transmission function $L_o(s) = G(s)P_o(s)$ that satisfies all the bounds and the stability contour.
- Step 11.** Based upon Steps 1 through 10, synthesize the prefilter $F(s)$.
- Step 12.** Simulate the system in order to obtain the time response data for each of the J plants.

The following sections will illustrate the design procedure step by step.

4.4 Minimum-phase system performance specifications

In order to apply the QFT technique, it is necessary to synthesize the desired model control ratio based upon the system's desired performance specifications in the time domain. For the minimum-phase LTI MISO system of Fig. 7, the control ratios for tracking and for disturbance rejection are, respectively,

$$T_R(s) = \frac{F(s)G(s)P(s)}{1 + G(s)P(s)} = \frac{F(s)L(s)}{1 + L(s)} = F(s)T(s) \quad \text{with } d_1(t) = d_2(t) = 0 \quad (7)$$

$$T_{D1} = \frac{P(s)}{1 + G(s)P(s)} = \frac{P}{1 + L} \quad \text{with } r(t) = d_2(t) = 0 \quad (8)$$

$$T_{D2} = \frac{1}{1 + G(s)P(s)} = \frac{1}{1 + L} \quad \text{with } r(t) = d_1(t) = 0 \quad (9)$$

4.4.1 Tracking models

The QFT technique requires that the desired tracking control ratios be modeled in the frequency domain to satisfy the required gain K_m and the desired time domain performance specifications for a step input. Thus, the system's tracking performance specifications for a simple second-order system are based upon satisfying some or all of the step forcing function figures of merit (FOM) for under-damped (M_p, t_p, t_s, t_r, K_m) and over-damped (t_s, t_r, K_m) responses, respectively. These are graphically depicted in Fig. 8. The time responses $y(t)_U$ and $y(t)_L$ in this figure represent the upper and lower bounds, respectively, of the tracking performance specifications; that is, an acceptable response $y(t)$ must lie between these bounds. The Bode plots of the upper bound B_U and lower bound B_L for $Lm T_R(j\omega)$ vs. ω are shown in Fig. 9.

It is desirable to synthesize the control ratios corresponding to the upper and lower bounds T_{RU} and T_{RL} , respectively, so that $\delta_R(j\omega_i)$ increases as ω_i increases above the 0-dB crossing frequency ω_{cf} (see Fig. 9b) of T_{RU} . This characteristic of $\delta_R(j\omega_i)$ simplifies the process of synthesizing the loop transmission $L_o(s) = G(s)P_o(s)$ as discussed in Sec. 4.13 of this chapter. To synthesize $L_o(s)$, it is necessary to determine the tracking bounds $B_R(j\omega_i)$ (see Sec. 4.9) which are obtained based upon $\delta_R(j\omega_i)$. This characteristic of $\delta_R(j\omega_i)$ ensures that the tracking bounds $B_R(j\omega_i)$ decrease in magnitude as ω_i increases.

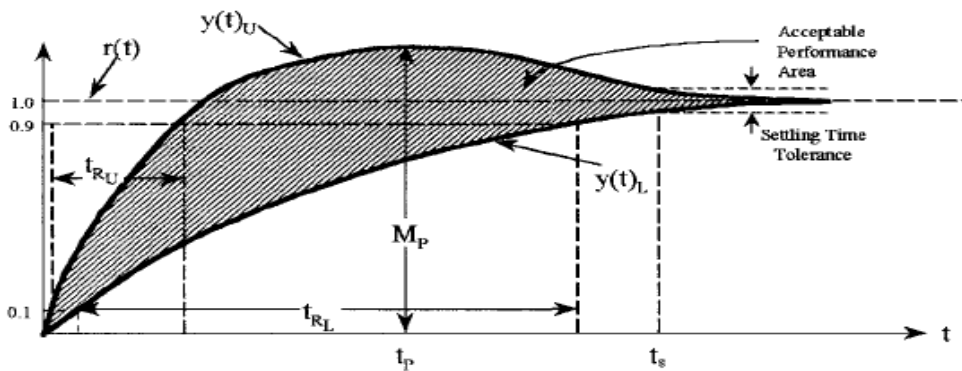
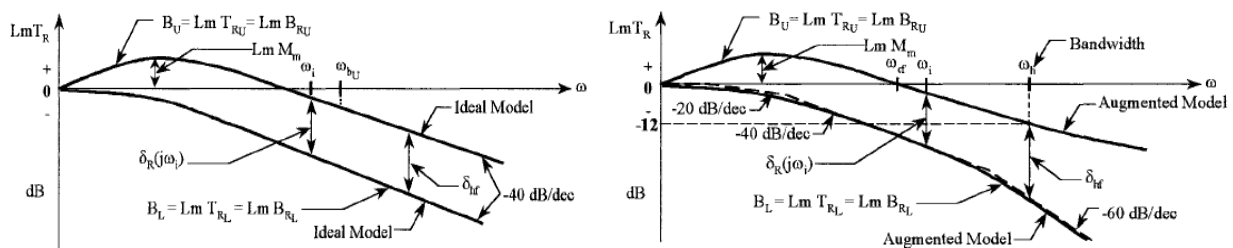


Fig. 8. System time domain tracking performance specifications



(a) Ideal simple second-order models (b) The augmented models

Fig. 9. Bode plots of T_R

An approach to the modeling process is to start with a simple second-order model of the desired control ratio T_{RU} having the form

$$T_{RU}(s) = \frac{\omega_n^2}{s^2 + 2\zeta\omega_n s + \omega_n^2} = \frac{\omega_n^2}{(s - p_1)(s - p_2)} \tag{10}$$

where $\omega_n^2 = p_1 p_2$ and $t_s \approx T_s = 4 / \zeta\omega_n = 4 / |\sigma_D|$ (the desired settling time). The control ratio $T_{RU}(s)$ of Eq. (10) can be represented by an equivalent unity-feedback system so that

$$T_{RU}(s) = \frac{Y(s)}{R(s)} = \frac{G_{eq}(s)}{1 + G_{eq}(s)} \tag{11}$$

where

$$G_{eq}(s) = \frac{\omega_n^2}{s(s + 2\zeta\omega_n)} \quad (12)$$

The gain constant of this equivalent Type1 transfer function $G_{eq}(s)$ is $K_1 = \lim_{s \rightarrow 0} [sG_{eq}(s)] = \omega_n / 2\zeta$.

The simplest over-damped model for $T_{RL}(s)$ is of the form

$$T_{RL}(s) = \frac{Y(s)}{R(s)} = \frac{K}{(s - \sigma_1)(s - \sigma_2)} = \frac{G_{eq}(s)}{1 + G_{eq}(s)} \quad (13)$$

where

$$G_{eq}(s) = \frac{\sigma_1\sigma_2}{s[s - (\sigma_1 + \sigma_2)]}$$

and $K_1 = -\sigma_1\sigma_2 / (\sigma_1 + \sigma_2)$. Selection of the parameters σ_1 and σ_2 is used to meet the specifications for t_s and K_1 .

Once the ideal models $T_{RL}(j\omega)$ and $T_{RL}(j\omega)$ are determined, the time and frequency response plots of Figs. 8 and 9a, respectively, can then be drawn. The high-frequency range in Fig. 9a is defined as $\omega \geq \omega_b$, where ω_b is the model BW frequency of B_u . In order to achieve the desired characteristic of an increasing magnitude of δ_r of B_u for $\omega_i > \omega_{cf}$, an increasing spread between B_u and B_L is required in the high-frequency range (see Fig. 9b), that is,

$$\delta_{hf} = B_u - B_L \quad (14)$$

must increase with increasing frequency. This desired increase in δ_r is achieved by changing B_u and B_L by augmenting T_{RL} with a zero [see Eq. (15)] as close to the origin as possible without significantly affecting the time response. This additional zero raises the curve B_u for the frequency range above ω_{cf} . The spread can be further increased by augmenting T_{RL} with a negative real pole [see Eq. (16)] which is as close to the origin as possible but far enough away not to significantly affect the time response. Note that the straight-line Bode plot is shown only for T_{RL} . This additional pole lowers B_L for this frequency range.

$$T_{RL}(s) = \frac{(\omega_n^2 / a)(s + a)}{s^2 + 2\zeta\omega_n s + \omega_n^2} = \frac{(\omega_n^2 / a)(s - z_1)}{(s - \sigma_1)(s - \sigma_2)} \quad (15)$$

$$T_{RL}(s) = \frac{K}{(s + a_1)(s + a_2)(s + a_3)} = \frac{K}{(s - \sigma_1)(s - \sigma_2)(s - \sigma_3)} \quad (16)$$

Thus, the magnitude of $\delta_r(j\omega_i)$ increases as ω_i increases above ω_{cf} .

In order to minimize the iteration process in achieving acceptable models for $T_{rL}(s)$ and $T_{rU}(s)$ which have an increasing $\delta_r(j\omega)$, the following procedure may expedite the design process: (a) first synthesize the second-order model of Eq. (15) containing the zero at $|z_1| = a \geq \omega_n$ that meets the desired FOM; and (b) then, as a first trial, select all three real poles of Eq. (16) to have the value of $|\sigma_3| = a_3 = \omega_n > a_2 = a_1 > |\sigma_D|$. For succeeding trials, if necessary, one or more of these poles are moved right and/or left until the desired specifications are satisfied. As illustrated by the slopes of the straight-line Bode plots in Fig. 9b, selecting the value of all three poles in the range specified above insures an increasing δ_r . Other possibilities are as follows: (c) the specified values of t_p and t_s for T_{rL} may be such that a pair of complex poles and a real pole need to be chosen for the model response. For this situation, the real pole must be more dominant than the complex poles, (d) depending on the performance specifications, $T_{rU}(s)$ may require two real poles and a zero "close" to the origin, i.e., select $|z_1|$ very much less than $|p_1|$ and $|p_2|$ in order to effectively have an under-damped response.

At high frequencies δ_{hf} (see Fig. 9b) must be larger than the actual variation in the plant, δ_p . For the case where $y(t)$, corresponding to T_{rU} , is to have an allowable "large" overshoot followed by a small tolerable undershoot, a dominant complex pole pair is not suitable for T_{rU} . An acceptable overshoot with no undershoot for T_{rU} can be achieved by T_{rU} having two real dominant poles $p_1 > p_2$, a dominant real zero ($z_1 > p_1$) "close" to p_1 , and a far off pole $p_3 \ll p_2$. The closeness of the zero dictates the value of M_p . Thus, a designer selects a pole-zero combination to yield the form of the desired time-domain response.

4.4.2 Disturbance rejection models

The simplest disturbance control ratio model specification is $|T_D(j\omega)| = |Y(j\omega / D(j\omega))| < a_p$, a constant, [the desired maximum magnitude of the output based upon a unit-step disturbance input]; i.e., for $d_1(t) : |y(t_p)| \leq a_p$, and for: $d_2(t) |y(t)| \leq a_p$ for $t \geq t_x$. Thus, the frequency domain disturbance specification is $Lm T_D(j\omega) < Lm a_p$ over the desired specified BW (see Fig. 10).

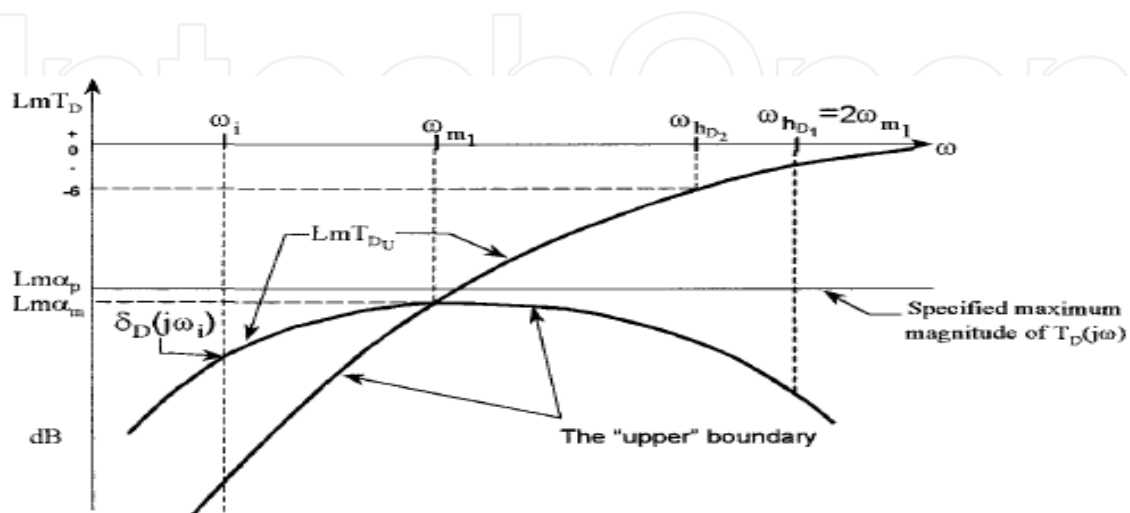


Fig. 10. Bode plots of disturbance models for $T_D(j\omega)$

4.5 J LTI plant models

The simple plant of Eq. (17)

$$P_i(s) = \frac{Ka}{s(s+a)} \quad (17)$$

where $K \in \{1,10\}$ and $a \in \{1,10\}$, is used to illustrate the MISO QFT design procedure. The region of plant parameter uncertainty may be described by J LTI plants, where $i = 1, 2, \dots, J$ which lie on its boundary.

4.6 Plant templates of $P_i(s), \Im P(j\omega_i)$

With $L = GP$, Eq. (7) yields

$$Lm T_R = Lm F + Lm \left[\frac{L}{1+L} \right] = Lm F + Lm T \quad (18)$$

The change in T_R due to the uncertainty in P , since F is LTI, is

$$\Delta(Lm T_R) = Lm T_R - Lm F = Lm \left[\frac{L}{1+L} \right] \quad (19)$$

The proper design of $L = L_o$ and F , must restrict this change in T_R so that the actual value of $Lm T_R$ always lies between B_u and B_l of Fig. 9b. The first step in synthesizing an L_o is to make NC templates which characterize the variation of the plant uncertainty for various values of ω_i , over a frequency range $\omega_x \leq \omega_i \leq \omega_{hR}$, where $\omega_x \leq \omega_{cf}$. For the plant of Eq. (17) the values $K = a = 1$ represent the lowest point of each of the templates $\Im P(j\omega_i)$ and may be selected as the nominal plant P_o for all frequencies.

4.7 Nominal plant

While any plant case can be chosen, it is a common practice to select, whenever possible, a plant whose NC point is always at the lower left corner of the template for all frequencies for which the templates are obtained.

4.8 U-contour (stability bound)

The specifications on system performance in the time domain (see Fig. 8) and in the frequency domain (see Fig. 9) identify a minimum damping ratio ζ for the dominant roots of the closed-loop system which corresponds to a bound on the value of $M_p \approx M_m$. On the NC this bound on $M_p \approx M_l$ (see Fig. 11) establishes a region which must not be penetrated by the templates and the loop transmission functions $L_i(j\omega)$ for all ω . The boundary of this region is referred to as the stability bound, the U-contour, because this becomes the dominating constraint on $L(j\omega)$. Therefore, the top portion, indicated by the coordinates efa, of the M_l contour becomes part of the U-contour. The formation of the U-contour is discussed in this section. For the two cases of disturbance rejection depicted in Fig. 7 the control ratios are, respectively, as given in Eqs. (8) and (9).

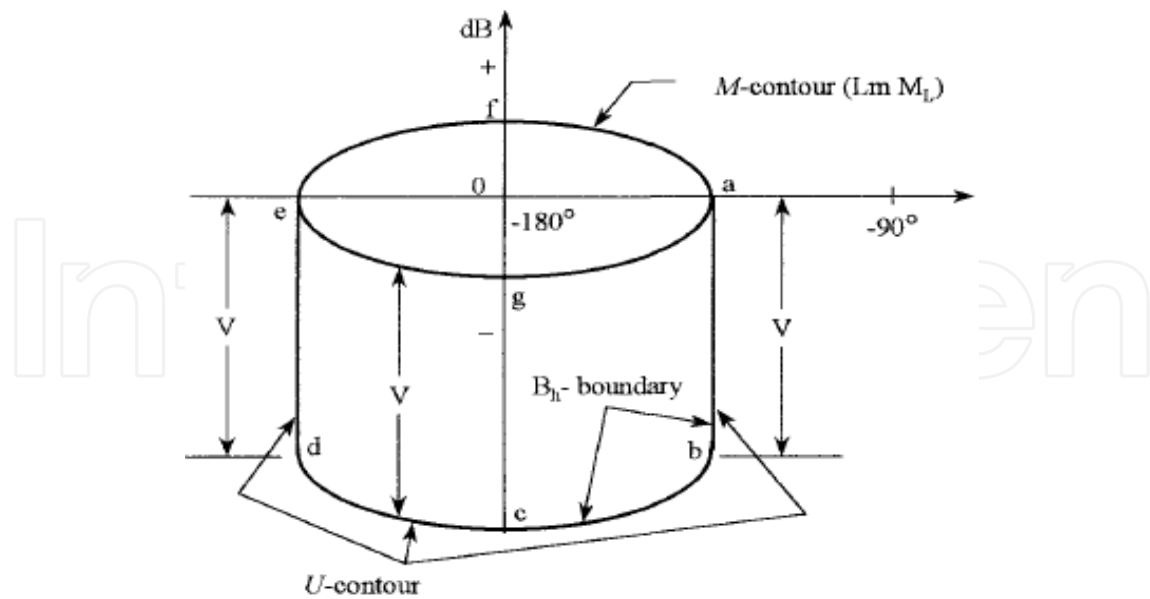


Fig. 11. U-contour construction (stability contour)

Thus, it is necessary to synthesize an $L_o(s)$ so that the disturbances are properly attenuated. For the present, only one aspect of this disturbance-response problem is considered, namely a constraint is placed on the damping ratio ζ of the dominant complex-pole pair of T_d nearest the ω -axis. This damping ratio is related to the peak value of

$$|T(j\omega)| = \left| \frac{L(j\omega)}{1+L(j\omega)} \right| \quad (20)$$

Therefore, it is reasonable to add the requirement

$$|T| = \left| \frac{L}{1+L} \right| \leq M_L \quad (21)$$

where M_L is a constant for all ω and over the whole range of φ parameter values. This results in a constraint on ζ of the dominant complex-pole pair of T_d . This constraint can therefore be transformed into a constraint on the maximum value T_{\max} of Eq. (20). This results in limiting the peak of the disturbance response. A value of M_L can be selected to correspond to the maximum value of T_R . Therefore, the top portion, efa as shown in Fig.11, of the M-contour on the NC, which corresponds to the value of the selected value of M_L , becomes part of the U-contour.

For a large class of problems, as $\omega \rightarrow \infty$, the limiting value of the plant transfer function approaches

$$\lim_{\omega \rightarrow \infty} [P(j\omega)] = \frac{K'}{\omega^\lambda}$$

where λ represents the excess of poles over zeros of $P(s)$.

4.9 Tracking bounds $B_R(j\omega_i)$

Consider the plot of $Lm P(j\omega)$ vs. $\angle P(j\omega)$ for a plant shown in Fig. 12 (the solid curve). With $G(s) = A = 1$ and $F(s) = 1$ in Fig. 7, $L = P$. The plot of $Lm L(j\omega)$ vs. $\angle L(j\omega)$ is tangent to the $M = 1$ dB curve with a resonant frequency $\omega_m = 1.1$. If $Lm M_m = 2$ dB is specified for $Lm T_R$, the gain A is increased, raising $Lm L(j\omega)$, until it is tangent to the 2-dB M -curve. For this example the curve is raised by $Lm A = 4.5$ dB ($G = A = 1.679$) and the resonant frequency is $\omega_m = 2.09$.

Now consider that the plant uncertainty involves only the variation in gain A between the values of 1 and 1.679. It is desired to find a cascade compensator $G(s)$, in Fig. 7, such that the specification $1 \text{ dB} < Lm M_m < 2 \text{ dB}$ is always maintained for this plant gain variation while the resonant frequency ω_m remains constant. This requires that the loop transmission $L(j\omega) = G(j\omega)P(j\omega)$ be synthesized so that it is tangent to an M -contour in the range of $1 \text{ dB} < Lm M < 2 \text{ dB}$ for the entire range of $1 < A < 1.679$ and the resultant resonant frequency satisfies the requirement $\omega_m = 2.09 + \Delta\omega_m$.

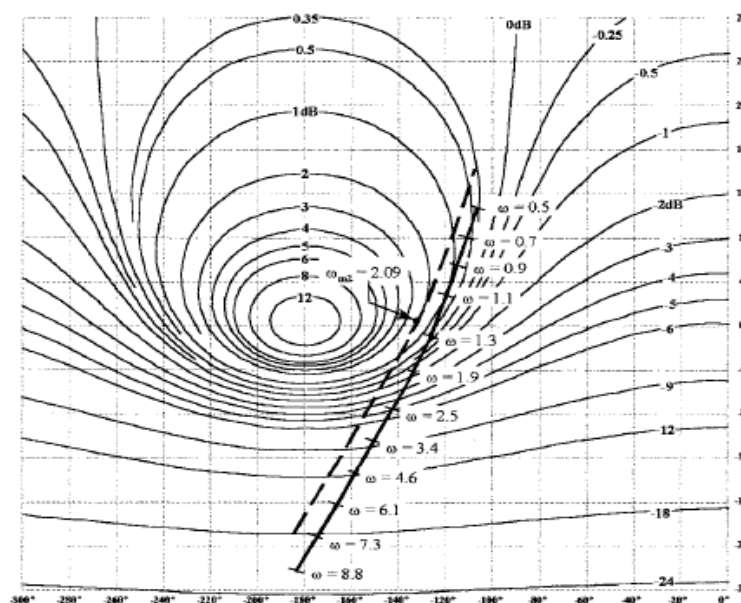


Fig. 12. Log magnitude-angle diagram

It is assumed for Eq. (19) that the compensators F and G are fixed (LTI), that is, they have negligible uncertainty. Thus, only the uncertainty in P contributes to the change in T_R given by Eq. (19). The solution requires that the actual $\Delta Lm T_R(j\omega_i) \leq \delta_R(j\omega_i)$ dB in Fig. 9b. Thus, it is necessary to determine the resulting constraint, or bound $B_R(j\omega_i)$, on $L(j\omega_i)$. The procedure is to select a nominal plant $P_o(s)$ and to derive the bounds on the resulting nominal loop transfer function $L_o(s) = G(s)P_o(s)$.

As an illustration, consider the plot of $Lm P(j2)$ vs. $\angle P(j2)$ for the plant of Eq. (17). As shown in Fig. 13, the plant's region of uncertainty $\Im P(j2)$ is given by the contour $ABCD$, i.e., $Lm P(j2)$ lies on or within the boundary of this contour. The nominal plant transfer function, with $K_o = 1$ and $a_o = 1$, is

$$P_o(s) = \frac{1}{s(s+1)} \tag{22}$$

and is represented in Fig. 13 by point A for $\omega = 2$ [-13.0 dB, -153.4°]. Note, once a nominal plant is chosen, it must be used for determining all the bounds $B_r(j\omega)$.

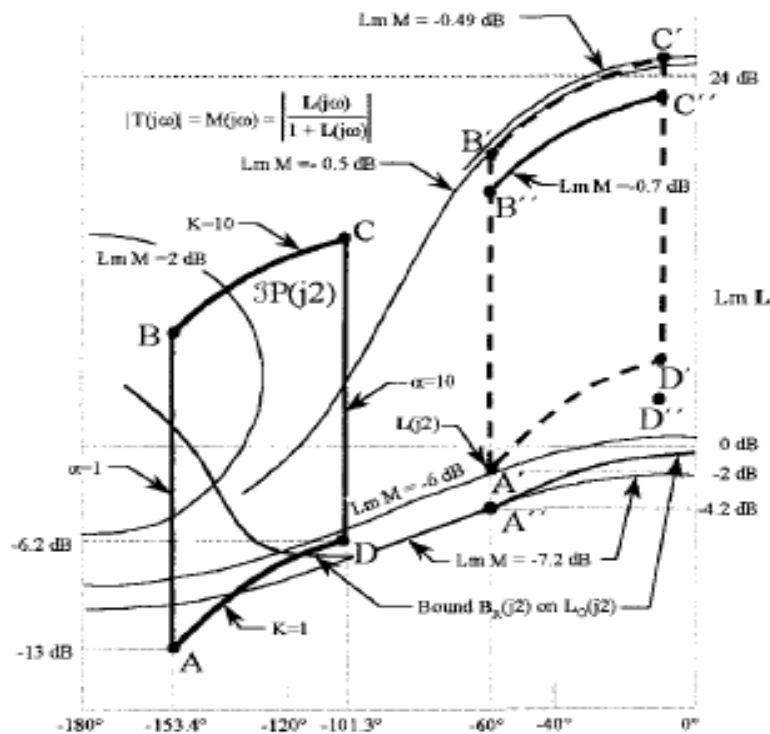


Fig. 13. Derivation of bounds $B_r(j\omega)$ on $L_r(j\omega)$ for $\omega = 2$

4.10 Disturbance bounds $B_d(j\omega)$: CASE 1

Two disturbance inputs are shown in Fig. 7. It is assumed that only one disturbance input exists at a time. Both cases are analyzed.

CASE 1 [$d_2(t) = D_0 u_{-1}(t), d_1(t) = 0$]

CONTROL RATIO. From Fig. 7, the disturbance control ratio for input $d_2(t)$ is

$$T_D(s) = \frac{1}{1+L} \tag{23}$$

Substituting $L = 1 / \ell$ into Eq. (23) yields

$$T_D(s) = \frac{\ell}{1+\ell} \tag{24}$$

this equation has the mathematical format required to use the NC. Over the specified BW it is desired that $|T_D(j\omega)| \ll 1$, which results in the requirement, from Eq.(24), that $|L(j\omega)| \gg 1$, i.e.,

$$T_d(j\omega) \approx \frac{1}{|L(j\omega)|} = |\ell(j\omega)|$$

DISTURBANCE RESPONSE CHARACTERISTIC. A time-domain tracking response characteristic based upon $r(t) = u_{-1}(t)$ often specifies a maximum allowable peak overshoot M_p . In the frequency domain this specification may be approximated by

$$|M_r(j\omega)| = |T_r(j\omega)| = \left| \frac{Y(j\omega)}{R(j\omega)} \right| \leq M_m \approx M_p \quad (25)$$

The corresponding time- and frequency-domain response characteristics, based upon the step disturbance forcing function $d_2(t) = u_{-1}(t)$, are, respectively,

$$|M_D(t)| = \left| \frac{Y(t)}{d(t)} \right| \leq \alpha_p \quad \text{for } t \geq t_s \quad (26)$$

and

$$|M_D(j\omega)| = |T_D(j\omega)| = \left| \frac{Y(j\omega)}{D(j\omega)} \right| \leq \alpha_m \approx \alpha_p \quad (27)$$

4.11 Disturbance bounds $B_D(j\omega)$: CASE 2

CASE 2 [$d_1(t) = D_0 u_{-1}(t), d_2(t) = 0$]

CONTROL RATIO. From Fig. 7, the disturbance control ratio for the input $d_1(t)$ is

$$T_D(j\omega) = \frac{P(j\omega)}{1 + G(j\omega)P(j\omega)} \quad (28)$$

Assuming point A of the template represents the nominal plant P_o . Eq. (28) is multiplied by P_o / P_o and rearranged as follows:

$$T_D = \frac{P_o}{P_o} \left[\frac{1}{\frac{1}{P} + G} \right] = \frac{P_o}{\frac{P_o}{P} + GP_o} = \frac{P_o}{\frac{P_o}{P} + L_o} = \frac{P_o}{W} \quad (29)$$

where

$$W = (P_o / P) + L_o \quad (30)$$

Thus Eq.(29) with $Lm T_D = \delta_D$ yields

$$Lm W = Lm P_o - \delta_D \quad (31)$$

DISTURBANCE RESPONSE CHARACTERISTICS. Based on Eq. (25), the time and frequency-domain response characteristics, for a unit-step disturbance forcing function, are given, respectively, by

$$|M_d(t)| = \left| \frac{y(t_p)}{d(t)} \right| = |y(t_p)| \leq \alpha_p \tag{32}$$

and

$$|M_d(j\omega)| = |T_d(j\omega)| = \left| \frac{Y(j\omega)}{D(j\omega)} \right| \leq \alpha_m \equiv \alpha_p \tag{33}$$

where t_p is the peak time.

4.12 The composite boundary $B_o(j\omega_i)$

The composite bound $B_o(j\omega_i)$ that is used to synthesize the desired loop transmission transfer function $L_o(s)$ is obtained in the manner shown in Fig. 14. The composite bound $B_o(j\omega_i)$, for each value of ω_i , is composed of those portions of each respective bound $B_R(j\omega_i)$ and $B_D(j\omega_i)$ that are the most restrictive. For the case shown in Fig. 14a the bound $B_o(j\omega_i)$ is composed of those portions of each respective bound $B_R(j\omega_i)$ and $B_D(j\omega_i)$ that have the largest values. For the situation of Fig. 14b, the outermost of the two boundaries $B_R(j\omega_i)$ and $B_D(j\omega_i)$ becomes the perimeter of $B_o(j\omega_i)$. The situations of Fig. 14 occur when the two bounds have one or more intersections. If there are no intersections, then the bound with the largest value or with the outermost boundary dominates. The synthesized $L_o(j\omega_i)$, for the situation of Fig. 14a, must be on or just above the bound $B_o(j\omega_i)$. For the situation of Fig. 14b the synthesized $L_o(j\omega_i)$ must not lie in the interior of the $B_o(j\omega_i)$ contour.

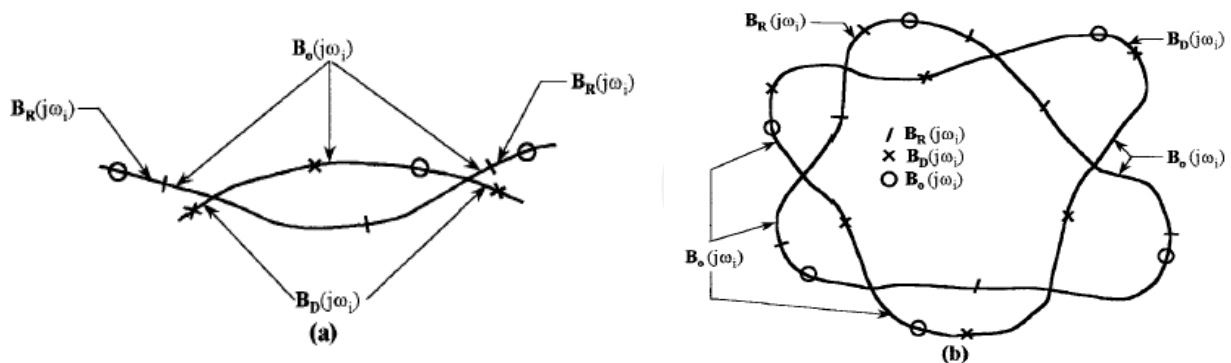


Fig. 14. Composite $B_o(j\omega_i)$

4.13 Shaping of $L_o(j\omega_i)$

A realistic definition of optimum in an LTI system is the minimization of the high-frequency loop gain K while satisfying the performance bounds. This gain affects the high-frequency response since $\lim_{\omega \rightarrow \infty} [L(j\omega)] = K(j\omega)^{-\lambda}$ where λ is the excess of poles over zeros assigned

to $L(j\omega)$. Thus, only the gain K has a significant effect on the high-frequency response, and the effect of the other parameter uncertainty is negligible. Also, the importance of minimizing the high-frequency loop gain is to minimize the effect of sensor noise whose spectrum, in general, lies in the high-frequency range.

For the plant of Eq. (17), the shaping of $L_o(j\omega)$ is shown by the dashed curve in Fig. 15. A point such as $Lm L_o(j2)$ must be on or above the curve labeled $B_o(j2)$. Further, in order to satisfy the specifications, $L_o(j\omega)$ cannot violate the U-contour. In this example a reasonable $L_o(j\omega)$ closely follows the U-contour up to $\omega = 40$ rad/sec and stays below it above $\omega = 40$ as shown in Fig 15. Additional specifications are $\lambda = 4$, i.e., there are 4 poles in excess of zeros, and that it also must be Type 1 (one pole at the origin). A representative procedure for choosing a rational function $L_o(s)$ which satisfies the above specifications is now described. It involves building up the function

$$L_o(j\omega) = L_{ok}(j\omega) = P_o(j\omega) \prod_{k=0}^w [K_k G_k(j\omega)] \quad (34)$$

where for $k = 0$, $G_o = 1 \angle 0^\circ$, and $K = \prod_{k=0}^w K_k$

In order to minimize the order of the compensator, a good starting point for "building up" the loop transmission function is to initially assume that $L_{o0}(j\omega) = P_o(j\omega)$ as indicated in Eq. (34). $L_o(j\omega)$ is built up term-by-term in order to stay just outside the U-contour in the NC of Fig. 15. The first step is to find the $B_o(j\omega_i)$ which dominates $L_o(j\omega)$.

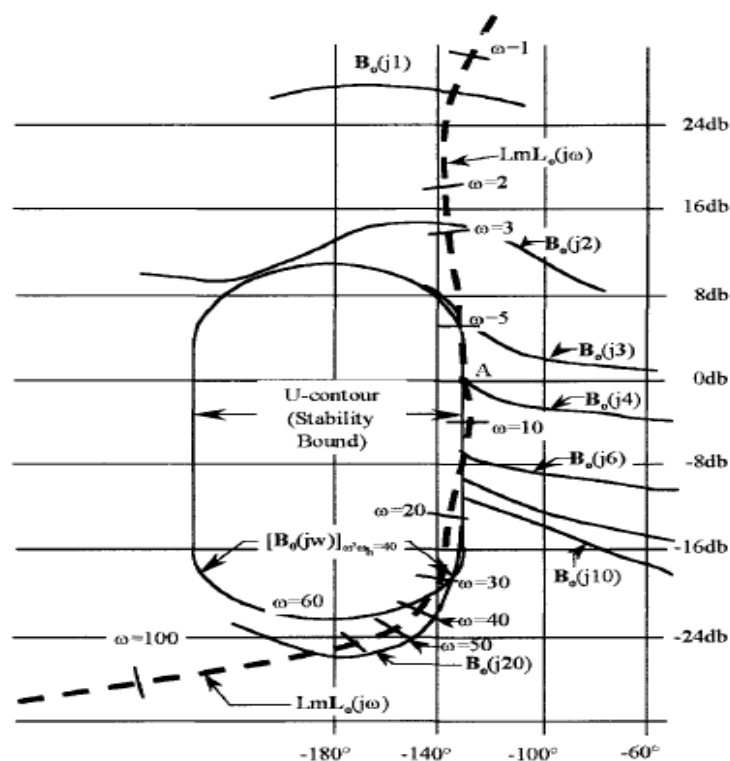


Fig. 15. Shaping of $L_o(j\omega)$ on the Nichols chart for the plant of Eq. (17)

4.14 Design of the prefilter $F(s)$

Design of a proper $L_o(s)$ guarantees only that the variation in $|T_R(j\omega)|$, i.e., ΔT_R , is less than or equal to that allowed. The purpose of the prefilter is to position $Lm T(j\omega)$ within the frequency domain specifications. For the example of this chapter the magnitude of the frequency response must be within the bounds B_U and B_L shown in Fig. 9b, which are redrawn in Fig. 16. A method for determining the bounds on $F(s)$ is as follows: Place the nominal point A of the ω_i plant template on the $L_o(j\omega_i)$ point of the $L_o(j\omega)$ curve on the NC (see Fig. 17). Traversing the template, determine the maximum $Lm T_{max}$ and minimum $Lm T_{min}$, values of

$$Lm T(j\omega_i) = \frac{L(j\omega_i)}{1 + L(j\omega_i)} \tag{35}$$

obtained from the M-contours. These values are plotted as shown in Fig. 16. The tracking control ratio is $T_R = FL / [1 + L]$ and

$$Lm T_R(j\omega_i) = Lm F(j\omega_i) + Lm T(j\omega_i) \tag{36}$$

The variations in Eqs. (35) and (36) are both due to the variation in P ; thus

$$\delta_L(j\omega_i) = Lm T_{max} - Lm T_{min} \leq \delta_R = B_U - B_L \tag{37}$$

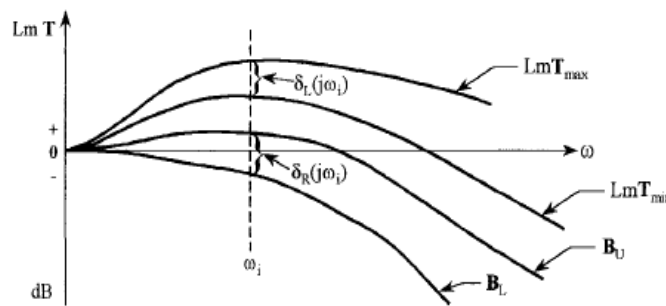


Fig. 16. Requirements on $F(s)$

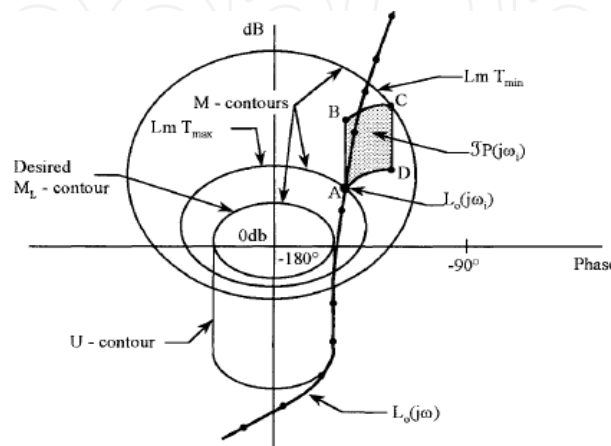


Fig. 17. Prefilter determination

If values of $L_o(j\omega)$, for each value ω_i , lie exactly on the tracking bounds $B_R(j\omega_i)$, then $\delta_L = \delta_R$. Therefore, based upon Eq. (36), it is necessary to determine the range in dB by which $Lm T(j\omega_i)$ must be raised or lowered to fit within the bounds of the specifications by use of the prefilter $F(j\omega_i)$. The process is repeated for each frequency corresponding to the templates used in the design of $L_o(j\omega)$. Therefore, in Fig. 18 the difference between the $Lm T_{RU} - Lm T_{max}$ and the $Lm T_{RL} - Lm T_{min}$ curves yields the requirement for $Lm F(j\omega)$, i.e., from Eq. (36).

$$Lm F(j\omega) = Lm T_R(j\omega) - Lm T(j\omega) \quad (38)$$

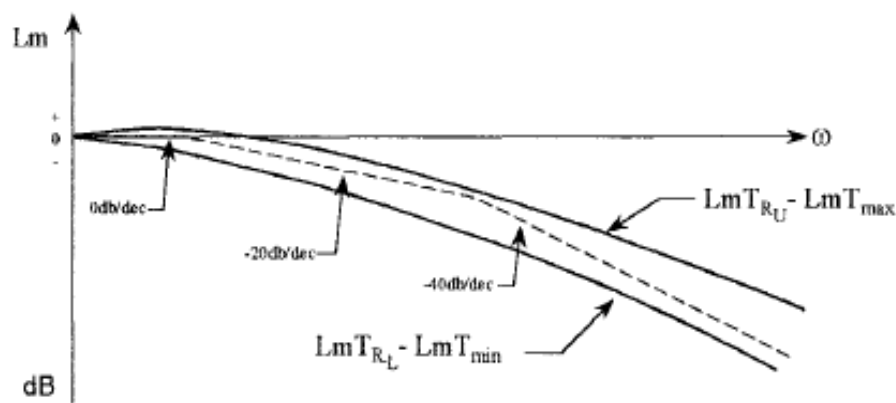


Fig. 18. Frequency bounds on the prefilter $F(s)$

The procedure for designing $F(s)$ is summarized as follows:

1. Use templates in conjunction with the $L_o(j\omega)$ plot on the NC to determine T_{max} and T_{min} for each ω_i . This is done by placing $\Im P(j\omega_i)$ with its nominal point on the point $Lm L_o(j\omega)$. Then use the M-contours to determine $T_{max}(j\omega_i)$ and $T_{min}(j\omega_i)$ (see Fig. 17).
2. Obtain the values of $Lm T_{RU}$ and $Lm T_{RL}$ for various values of a , from Fig. 9b.
3. From the values obtained in steps 1 and 2, plot $[Lm T_{RU} - Lm T_{max}]$ and $[Lm T_{RL} - Lm T_{min}]$ vs. ω as shown in Fig. 18.
4. Use straight-line approximations to synthesize an $F(s)$ so that $Lm F(j\omega)$ lies within the plots of step 3. For step forcing functions the resulting $F(s)$ must satisfy

$$\lim_{s \rightarrow 0} [F(s)] = 1 \quad (39)$$

4.15 Basic design procedure for a MISO system

The basic concepts of the QFT technique are explained by means of a design example. The system configuration shown in Fig. 7 contains three inputs. The first objectives are to track a step input $r(t) = u_{-1}(t)$ with no steady-state error and to satisfy the performance specifications of Fig. 8. An additional objective is to attenuate the system response caused by

external step disturbance inputs $d_1(t)$ and $d_2(t)$. An outline of the basic design procedure for the QFT technique, as applied to a minimum-phase plant, is as follows:

1. Synthesize the tracking model control ratio $T_r(s)$ in the way described in Sec. 4.4, based upon the desired tracking specifications (see Figs. 8 and 9b).
2. Synthesize the disturbance-rejection model control ratios $T_d(s)$ in the manner described in Sec. 4.10 based upon the disturbance-rejection specifications.
3. Obtain templates of $P(j\omega_i)$ that pictorially describe the plant uncertainty on the Nichols chart for the desired pass-band frequency range.
4. Select a nominal plant from the set of Eq. (5) and denote it as $P_o(s)$.
5. Determine the U-contour based upon the specified values of $\delta_r(j\omega_i)$ for tracking, M_L for disturbance rejection, and V for the universal high frequency boundary (UHFB) in conjunction with steps 6 through 8.
6. Use the data of steps 2 and 3 and the values of $\delta_d(j\omega_i)$ (see Fig. 10) to determine the disturbance bound $B_d(j\omega_i)$ on the loop transmission $L_d(j\omega_i) = G(j\omega_i)P_o(j\omega_i)$. For minimum-phase systems this requires that the synthesized loop transmission $Lm L_d(j\omega_i)$ must be on or above the curve for $Lm B_d(j\omega_i)$ on the Nichols diagram (see Fig. 15 assuming $B_d = B_o$).
7. Determine the tracking bound $B_r(j\omega_i)$ on the nominal transmission $L_o(j\omega_i) = G(j\omega_i)P_o(j\omega_i)$, using the tracking model (step 1), the templates $P(j\omega_i)$ (step 3), the values of $\delta_r(j\omega_i)$ (see Fig. 9b), and M_L [see Eq.(21)]. For minimum-phase systems this requires that the synthesized loop transmission satisfy the requirement that $Lm L_o(j\omega_i)$ is on or above the curve for $Lm B_r(j\omega_i)$ on the Nichols diagram.
8. Plot curves of $Lm B_r(j\omega_i)$ versus $\phi_r = \angle B_r(j\omega_i)$ and $Lm B_d(j\omega_i)$ versus $\phi_d = \angle B_d(j\omega_i)$ on the same NC. For a given value of ω_i at various values of the angle ϕ , select the value of $Lm B_d(j\omega_i)$ or $Lm B_r(j\omega_i)$, whichever is the largest value (termed the "worst" or "most severe" boundary). Draw a curve through these points. The resulting plot defines the overall boundary $Lm B_o(j\omega_i)$ vs. ϕ . Repeat this procedure for sufficient values of ω_i .
9. Design $L_o(j\omega_i)$ to be as close as possible to the boundary value $B_o(j\omega_i)$ by selecting an appropriate compensator transfer function $G(j\omega)$. Synthesize an $L_o(j\omega) = G(j\omega)P_o(j\omega)$ using the $Lm B_o(j\omega_i)$ boundaries and U-contour so that $Lm L_o(j\omega_i)$ is on or above the curve for $Lm B_o(j\omega_i)$ on the Nichols diagram.
10. Based upon the information available from steps 1 and 9, synthesize an $F(s)$ those results in a $Lm T_r$ [Eq. (7)] vs. ω that lies between B_u and B_l of Fig. 9b.
11. Obtain the time-response data for $y(t)$: (a) with $d(t) = u_{-1}(t)$ and $r(t) = 0$ and (b) with $r(t) = u_{-1}(t)$ and $d(t) = 0$ for sufficient points around the parameter space describing the plant uncertainty.

5. Robust QFT flight control design for a certain UAV

5.1 Introduction

Unmanned Aerial Vehicles (hereafter referred as UAVs) play a very important role in modern war. Whereas flight stability of UAVs is easily affected by airflow, model perturbation and other uncertainty. To enhance flight stability and robustness of UAVs,

H_∞ control, QFT technique, linear quadratic Gaussian (LQG) have been applied to UAVs' flight control system at present. Comparatively, QFT can take uncertainty's scopes and performance requirements into account, analyze and design robust controller on Nichols chart quantitatively in order to make the open-loop frequency curve comply with boundary conditions and have robust stability and performance robustness.

QFT has been widely used in aerospace field and is mature for robust controller design of LTI/SISO system. But QFT design for MIMO system still faces many difficulties. In view of the characteristics of a certain small UAV which used in tracking and surveillance, a novel QFT controller design method for the UAV's lateral motion is introduced in this section.

5.2 QFT design for MIMO systems

5.2.1 Overview

The QFT design for MIMO systems is based upon the mathematical means which results in the representation of a MIMO control system by m^2 MISO equivalent control systems. The highly structured uncertain LTT MIMO plant has the following features:

1. The synthesis problem is converted into a number of single-loop problems, in which structured parameter uncertainty, external disturbance, and performance tolerances are derived from the original MIMO problem. The solutions to these single-loop problems are guaranteed to work for the MIMO plant. It is not necessary to consider the system characteristic equation.
2. The design is tuned to the extent of the uncertainty and the performance tolerances. The design for a MIMO system, as stated previously, involves the design of an equivalent set of MISO system feedback loops.

The design process for these individual loops is the same as the design of a MISO system described in previous sections.

Pure mathematical transformation method used in QFT design for MIMO systems tends to cause a larger super-margin design and is very complicated when system is of higher order. Comparatively, Basically Non-interacting (hereafter referred as BNIA) is commonly used in practical applications. Note that principle of BNIA, which will be negligible here, can be found in references of this chapter.

5.2.2 Non-interacting (BNIA) loops

A BNIA loop is one in which the output $y_k(s)$ due to the input $r_j(s)$ is ideally zero. Plant uncertainty and loop interaction (cross-coupling) makes the ideal response unachievable. Thus, the system performance specifications describe a range of acceptable responses for the commanded output and a maximum tolerable response for the uncommanded outputs. The uncommanded outputs are treated as cross-coupling effects.

For an LTI plant having no parameter uncertainty, it is possible to essentially achieve zero cross-coupling effects, i.e., the output $y_k \approx 0$. This desired result can be achieved by post multiplying P by a matrix W to yield:

$$P_n = PW = [p_{ijn}] \quad \text{where } p_{ijn} = 0 \text{ for } i \neq j$$

resulting in a diagonal P_n matrix for P representing the nominal plant case in the set φ . With plant uncertainty the off-diagonal terms of P_n will not be zero but "very small" in comparison to P , for the nonnominal plant cases in φ . In some design problems it may be necessary or desired to determine a P_n upon which the QFT design is accomplished. Doing this minimizes the effort required to achieve the desired BW and minimizes the cross-coupling effects.

5.3 QFT design and simulation for a certain UAV's lateral motion

QFT approach for MIMO system will be applied to a certain UAV's lateral motion in this section.

5.3.1 Mathematical model of the UAV

State equation of the UAV is generally expressed as:

$$\begin{cases} \dot{x}(t) = Ax(t) + Bu(t) \\ y(t) = Cx(t) \end{cases} \quad (40)$$

where $X = [\beta \ p \ \gamma \ \phi \ \delta_a \ \delta_r]^T$; $u = [\delta_{rc} \ \delta_{ac}]^T$; $Y = [\beta \ p \ \gamma \ \phi]^T$; β is sideslip angle, p is roll angle rate, γ is yaw angle rate, ϕ is roll angle, δ_a is aileron deflection angle, δ_r is rudder deflection angle, δ_{rc} is rudder deflection angle command input, A, B, C are system matrix, input matrix and input-output matrix respectively. By way of wind tunnel test and mathematic method, matrices A, B and C in eqs.(40) for the small UAV can be derived.

5.3.2 System decomposition

The UAV's lateral state equation described in Eq.(40) has two inputs and four outputs. According to QFT approach for MIMO system, we decompose Eq.(40) into two MISO subsystems using BNIA, one is yaw loop (loop I) subsystem, the other is roll loop (loop II) subsystem. QFT control structures of both loops are given in Fig.19 and Fig.20.

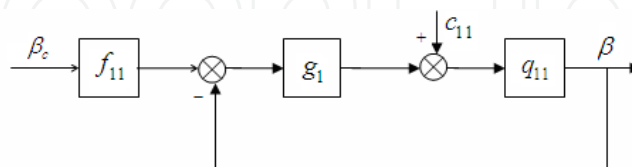


Fig. 19. QFT control structure of loop I

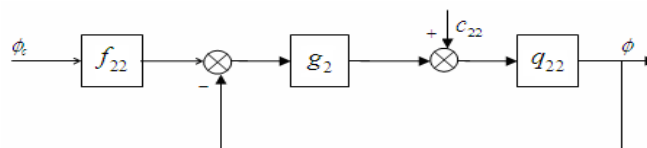


Fig. 20. QFT control structure of loop II

where β_c, ϕ_c are sideslip angle input and roll angle input respectively; g_1, g_2 are QFT controllers; f_{11}, f_{22} are QFT prefilters; c_{11}, c_{22} are disturbance inputs; q_{11}, q_{22} is controlled plants.

Decomposed state equation has relationship with that of the original system as follows:

$$A_c = A, B_c = B, C_c = \begin{bmatrix} 1 & 0 & 0 & 0 \\ 0 & 0 & 0 & 1 \end{bmatrix} C$$

Transfer function matrices P of decomposed plant can be easily derived as

$$P = C_c (sI - A_c)^{-1} B_c = \begin{bmatrix} p_{11} & p_{12} \\ p_{21} & p_{22} \end{bmatrix}$$

where p_{11} is the transfer function from δ_{rc} to β ; p_{22} represents the transfer function from δ_{ac} to ϕ ; p_{12} is the transfer function from δ_{rc} to ϕ , p_{21} represents the transfer function from δ_{ac} to β .

Next, we adopt 5 flight states to develop the QFT controllers of both loops.

5.3.3 QFT design for loop I

For loop I, we ensure $g_1(s)$ and $f_{11}(s)$ meet requirements of robust stability when β_c acts as command input and c_{11} as disturbance input. Besides, both subsystems should own ideal tracking performance and preferable noise restraint capability.

1. **Selection of Performance Indices.** Tracking performances indices of sideslip angle are overshoot $\sigma\% \leq 2\%$, settling time $t_s \leq 6\%$. Given the original model of upper tracking boundary is

$$T_{RU}(j\omega) = \frac{\omega_n^2}{s^2 + 2\zeta\omega_n s + \omega_n^2} \quad (41)$$

According to $\sigma\%$ and t_s , damping ratio ζ and natural oscillation frequency ω_n is adopted as 0.78 and 0.8978. Add a zero ($z=-1$) as close to the origin as possible without significantly affecting the time response (see Sec.4.4.1). This additional zero raises tracking boundary curve above ω_{cf} , the final transfer function of tracking curve's upper boundary is

$$T_{RU}(j\omega) = \frac{0.806(s+1)}{s^2 + 1.4s + 0.806} \quad (42)$$

the lower boundary original model of tracking curve as

$$T_{RL}(j\omega) = \frac{0.9}{s+0.9} \quad (43)$$

Adding two poles ($p_1=-1, p_2=-4$), which locate in left half s-plane to ensure stability of T_{RL} and are as close to the origin as possible but far enough away not to significantly affect the time response (see Sec.4.4.1), to eq. (43) to make lower tracking boundary separate from

upper tracking boundary when upper tracking boundary cross over 0 dB line, then the final lower boundary transfer function is

$$T_{RL}(j\omega) = \frac{3.6}{(s+0.9)(s+1)(s+4)} \quad (44)$$

Stability performance index and robust performance index are respectively

$$\left| \frac{q_{11}(s)g_1(s)}{1+q_{11}(s)g_1(s)} \right| \leq 1.1$$

and

$$\left| \frac{q_{11}(s)}{1+q_{11}(s)g_1(s)} \right| \leq 0.1$$

Corresponding minimum amplitude margin and phase margin are respectively

$$K_m = 1 + \frac{1}{\mu} = 1.9091 = 5.5155 \text{dB}$$

and

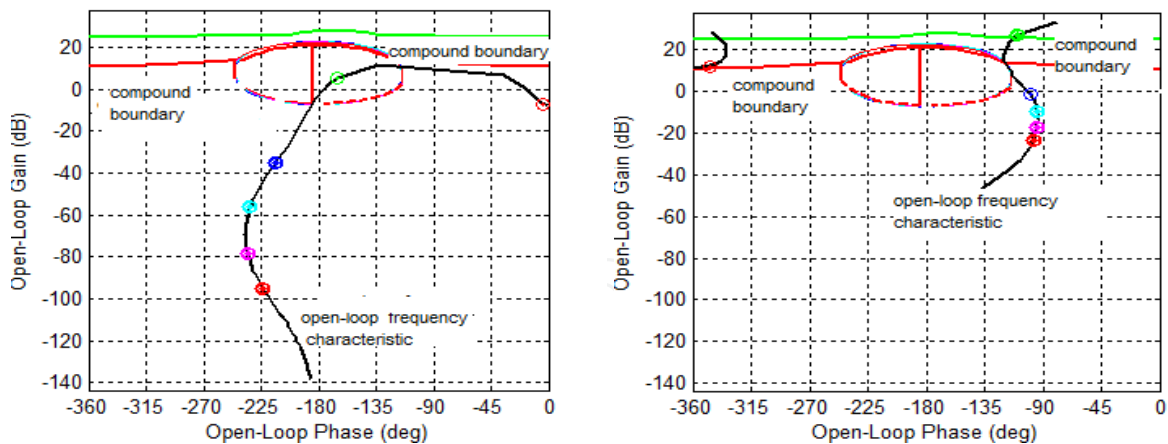
$$\Phi_m = 180^\circ - \theta, \theta = \cos^{-1}(0.5 / \mu^2 - 1) = 54.062^\circ$$

2. **Plant Template and Border Calculation for Loop I.** According to the requirements of performance index, generate the tracking response boundary, robust stability boundary and inference rejection boundary in Nichols chart.
3. **Controller and Prefilter Design for Loop I.** In Fig. 21(a), the open-loop frequency characteristics curve (noted by black solid line) of the nominal plant (corresponding to $G(s)=1$) and the compound boundary (the region embraced by green and red solid line) are drawn up in Nichols chart. Apparently, the open-loop frequency curve locates under tracking performance boundary curve, open-loop frequency characteristics curve cross over the instability boundary (red solid ring line in Fig. 21(a)) which make the MISO system of loop I instable or unsatisfactory for corresponding performance requirements. So, it is necessary to enlarge the controller gain and introduce into dynamic compensation element to shape the open loop frequency characteristic curve to ensure shaped open-loop frequency characteristic meet the requirements of stability and dynamic performance indicis. Using MATLAB QFT toolbox, we get

$$g_1(s) = \frac{8.855(s/2.045+1)(s/8.68+1)}{(s/113.5+1)(s/907.9+1)} \quad (45)$$

$$f_{11}(s) = \frac{1.275}{s/0.6+1} \quad (46)$$

The open-loop frequency characteristics curve with $G(s)$ is shown in Fig.21 (b). Clearly, the shaped curve does not cross over the instability region (red solid ring line), i.e. the shaped system is stable. Besides, the characteristic of tracking boundary is met.



(a) Open-loop frequency response when $G(s) = 1$ (b) Open-loop frequency response with controller

Fig. 21. Open loop frequency characteristics in Nichols Chart

4. **Verification and Simulation for Loop I.** Closed-loop system stability margin analysis curve, inference rejection boundary analysis curves and tracking boundary analysis curves in loop I are given in Fig.22, Fig.23 and Fig.24. Clearly, the stability margin curve, inference rejection boundary curve and tracking boundary curve are all under the stability performance index curve, the performance index curve and between the upper and lower boundaries of tracking curves. Obviously, Closed-loop control system satisfies the performance requirements in loop I.

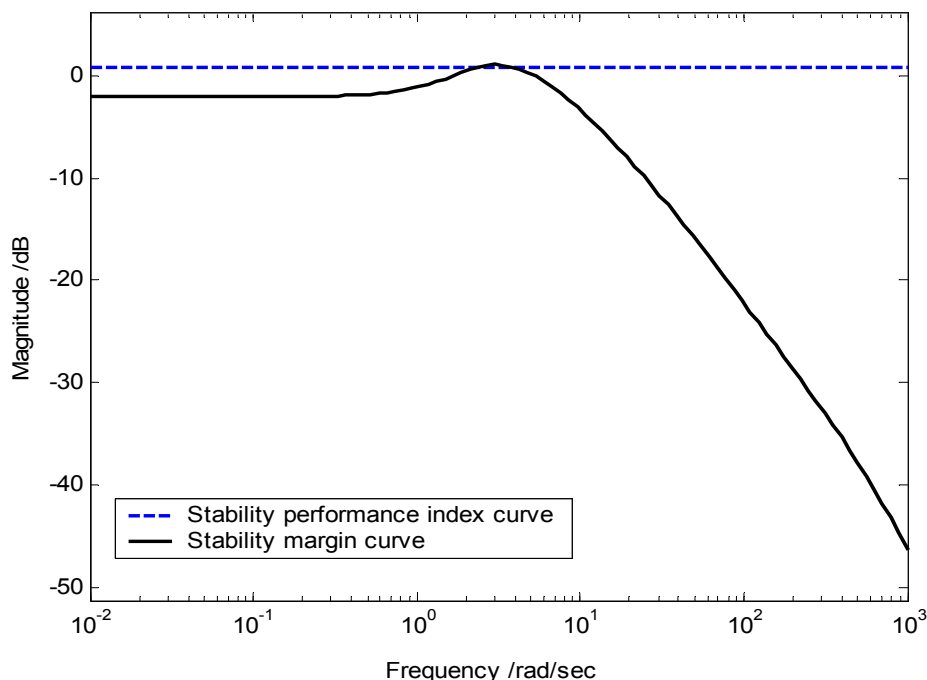


Fig. 22. Stability margin

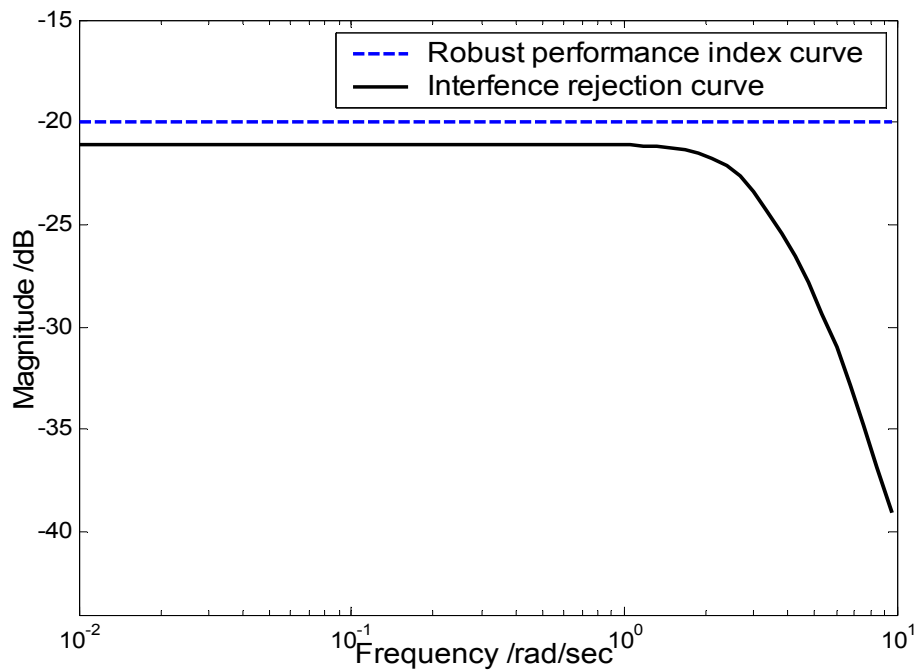


Fig. 23. Disturbance rejection boundary

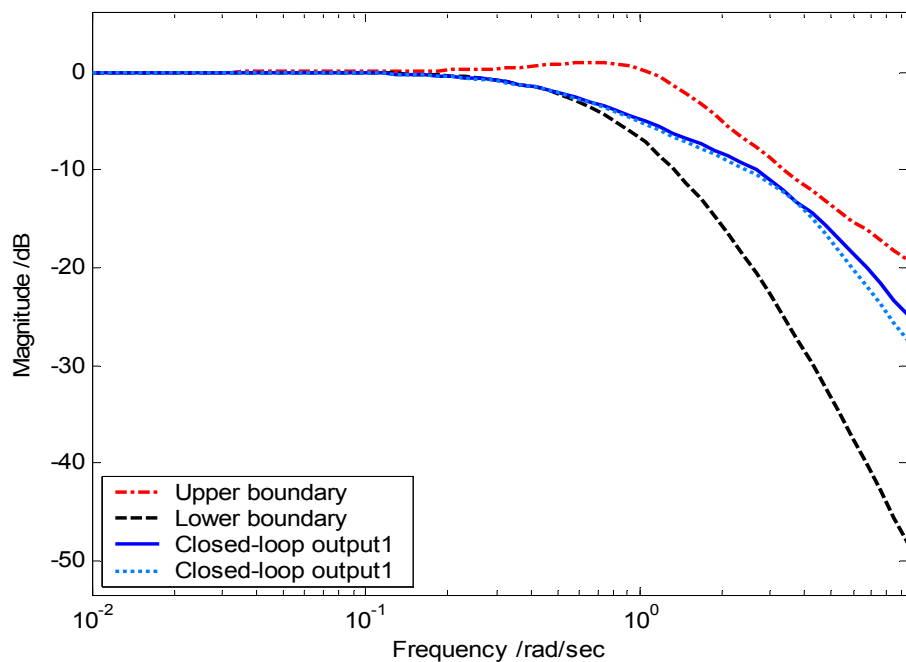


Fig. 24. Tracking boundary

The time-domain simulation results of closed-loop system under 5 design envelopes are shown in Fig.25 and Fig.26. The unit step-response of sideslip angle lies between the upper and lower boundary response curve; the unit step-response of disturbance input are located under the given boundary. Apparently, the closed-loop system satisfies the requirements of robust stability and tracking boundary requirements, and owns strong disturbance rejection capability.

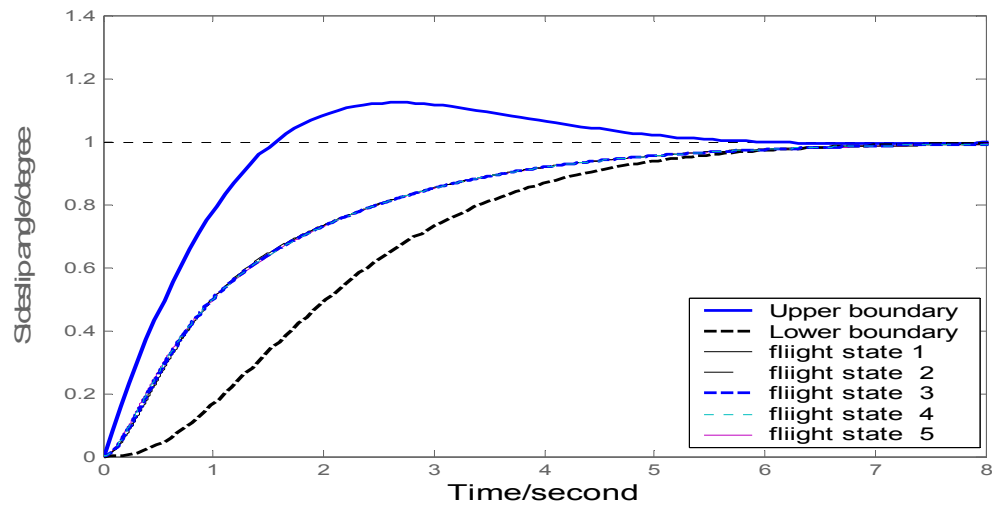


Fig. 25. The unit step response of β

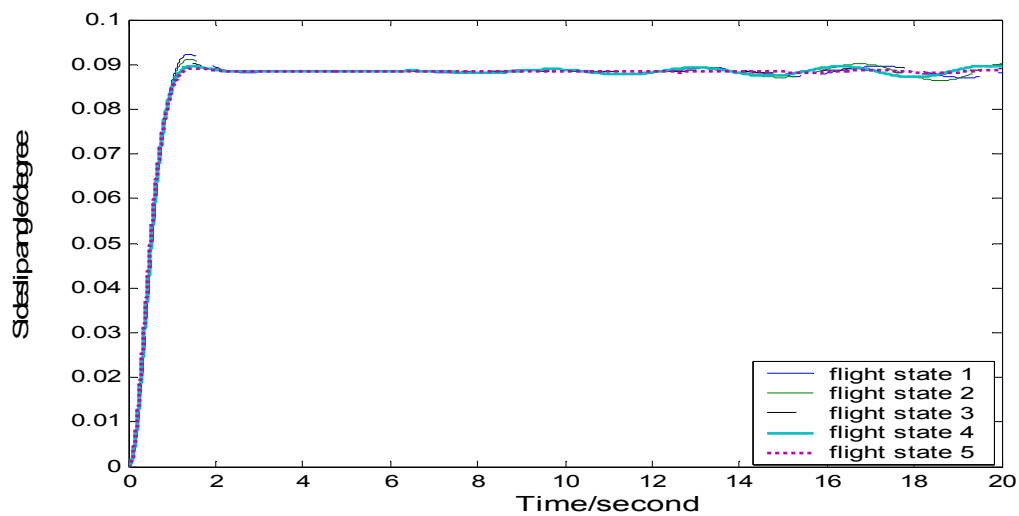


Fig. 26. The unit step response of β with disturbance

5.3.4 QFT design for loop II

QFT design for loop II is similar to that for loop I.

1. **Selection of Performance Indices.** Tracking performance indices of roll angle is overshoot $\sigma\% \leq 5\%$ and settling time $t_s \leq 12s$, the upper and lower boundary tracking curve are respectively

$$T_{RU}(j\omega) = \frac{0.25(1.7s + 1)}{s^2 + 0.78s + 0.25} \quad (47)$$

$$T_{RL}(j\omega) = \frac{3.6}{(s+0.9)(s+1)(s+4)} \quad (48)$$

Stability performance index and robust performance index are defined as

$$\left| \frac{q_{22}(s)g_2(s)}{1+q_{22}(s)g_2(s)} \right| \leq \mu = 1.1 \text{ and } \left| \frac{q_{22}(s)}{1+q_{22}(s)g_2(s)} \right| \leq 0.1$$

Minimum amplitude margin and phase margin are 5.5155B and 54.062° respectively.

2. Controller and Prefilter Design for Loop II.

Similar to loop I, using MATLAB QFT toolbox, we can get

$$g_2(s) = \frac{11.8(s/27.94+1)(s/1.18+1)}{(s/1280+1)(s/1926+1)} \quad (49)$$

$$f_{22}(s) = \frac{1.01}{(s/0.7+1)} \quad (50)$$

3. **Verification and Simulation for loop II.** Closed-loop system satisfies requirements of robust stability and tracking boundary requirements and owns strong disturbance rejection capability.

5.3.5 Performance analysis of QFT controller for the UAV's lateral motion

QFT control structure for the UAV's lateral motion is shown in Fig.27. Given β_c and ϕ_c are 0, the initial value of ϕ is 5°, the initial sideslip angle β is 1°, substitute the UAV's lateral state equation, $g_1(s), f_{11}(s), g_2(s), f_{22}(s)$, models of rudder and ailerons into Fig.27. The simulation results are shown in Fig.28 and Fig.29. The overshoot of β is about 0.064 and settling time is about 1 second. The settling time of yaw angle rate, roll angle rate and roll angle are all about 0.1 second. Besides, the initial value of sideslip angle almost have no influence in roll angle response, the settling time of yaw angle rate, roll angle rate is no more than 1 second. Clearly, QFT controller for the UAV's lateral motion satisfies the requirements of performance indices, own better flight stability and robustness.

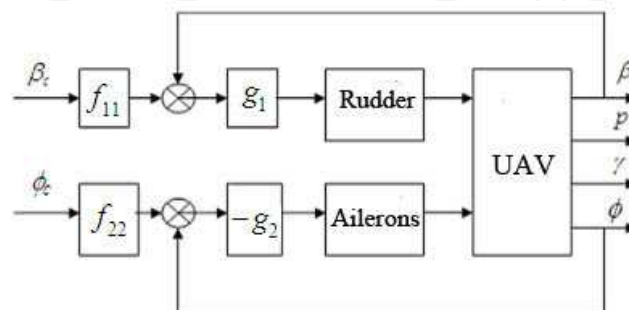
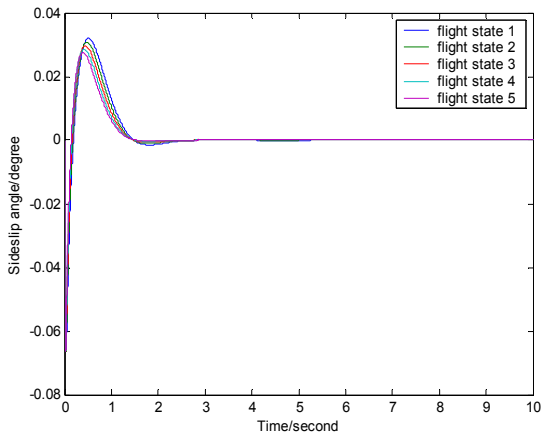
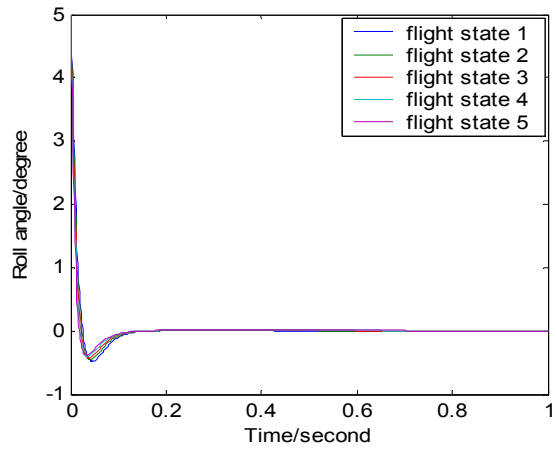


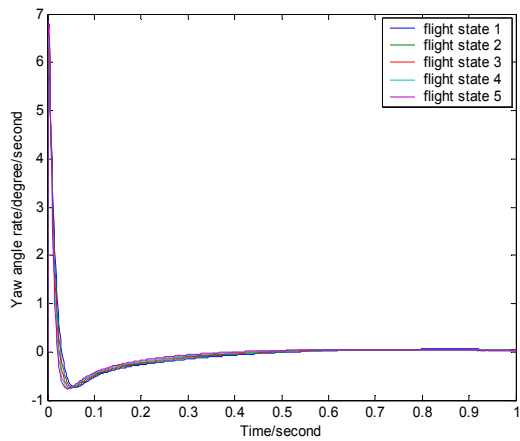
Fig. 27. QFT control structure for the UAV's lateral motion



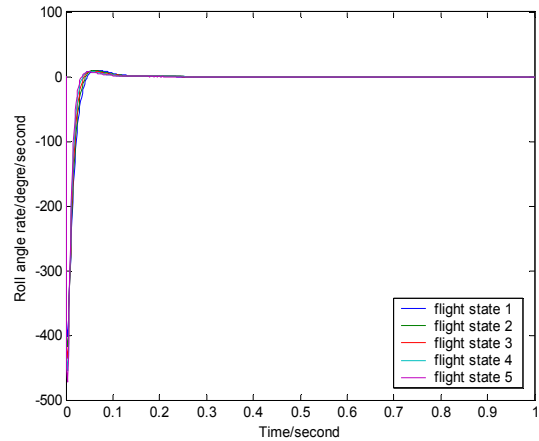
(a) Sideslip angle



(b) Roll angle

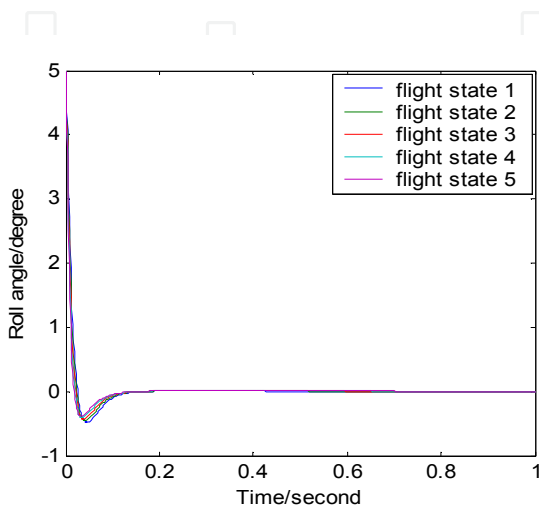


(c) Yaw angle rate

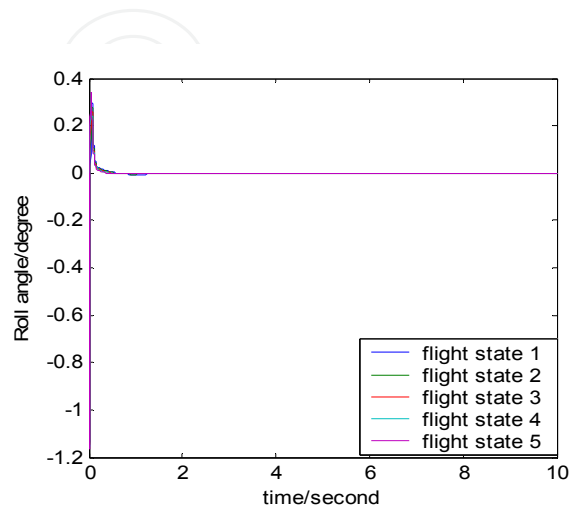


(d) Roll angle rate

Fig. 28. Responses of sideslip angle, roll angle, yaw angle rate and roll angle rate when $\phi_0 = 5^\circ$



(a) Sideslip angle



(b) Roll angle

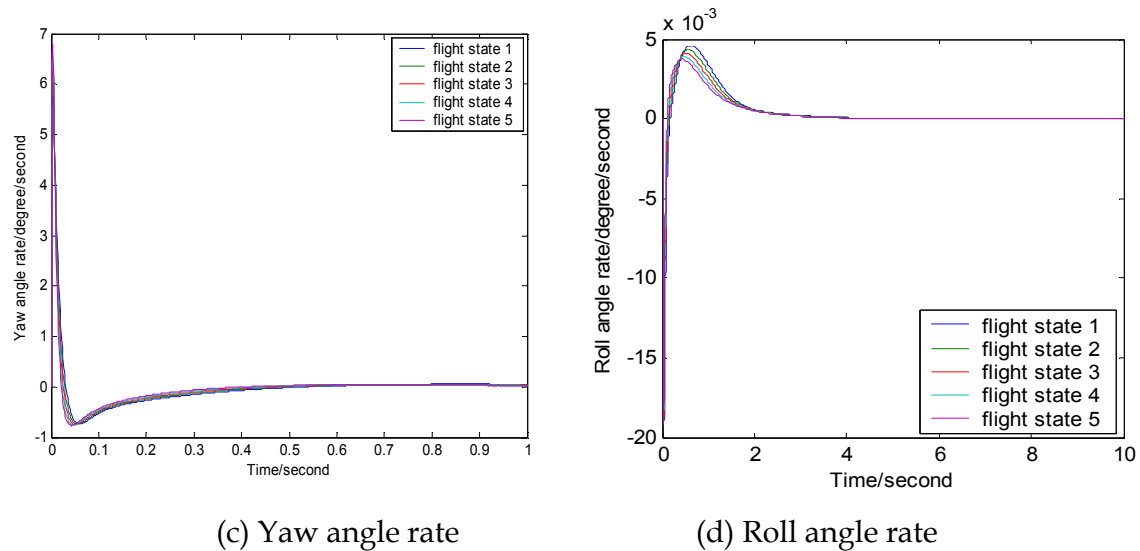


Fig. 29. Responses of sideslip angle, roll angle, yaw angle rate and roll angle rate when $\beta_0 = 1^\circ$

6. Summary

This chapter is devoted to presenting an overview and in-depth expression of QFT in order to enhance the understanding and appreciation of the power of the QFT technique. Then, A QFT design of robust controller for a certain UAV's lateral motion, which is a MIMO system, is proposed base on BNIA principle in order to show how to apply QFT in flight control system of UAVs. Meantime, the simulation results show that the QFT controller own better robust stability and superior dynamic characteristics which verify the validity of presented method.

7. Symbols & terminology

T_R Acceptable command or tracking input-output responses

\mathfrak{T}_R A set of T_R

T_D Acceptable disturbance input-output responses

\mathfrak{T}_D A set of T_D

P MISO plant with uncertainty

φ A set of P

MIMO Multiple-input multiple-output; more than one tracking and/or external disturbance inputs and more than one output

MISO Multiple-input single-output; a system having one tracking input, one or more external disturbance inputs, and a single output

$B_d(j\omega_i), B_k(j\omega_i), B_o(j\omega_i)$ The disturbance, tracking, and optimal bounds on $L(j\omega_i)$ for the MISO system

ω_h The frequency bandwidth

$\delta_i(j\omega)$ The magnitude variation due to the plant parameter uncertainty

Lm Log magnitude

LTI Linear-time-invariant

FOM figure of merit

ω_b The symbol for bandwidth frequency of the models

ω_m The resonant frequency

$\omega_\phi, \omega_{\phi_i}$ Phase margin frequency for a MISO system and for the i^{th} loop of a MIMO system, respectively

ω_s Sampling frequency

$R, R = \{r_i\}$ The tracking input for a MISO system and the tracking input vector for a MIMO system, respectively

$B_u = Lm T_{rU}$ The Lm of the desired tracking control ratio for the upper bound of the MISO system

$B_L = Lm T_{rL}$ The Lm of the desired tracking control ratio for the lower bound of the MISO system

B_s Stability bounds for the discrete design

$\delta_d(j\omega_i)$ The (upper) value of $Lm T_d(j\omega_i)$ for MISO system

$\delta_{hf}(j\omega_i)$ The dB difference between the augmented bounds of B_u and B_L in the high frequency range for a MISO system

$\delta_r(j\omega_i)$ The dB difference between B_u and B_L for a given frequency ω , for a MISO system

$F, F = \{f_{ij}\}$ The prefilter for a MISO system and the mxm prefilter matrix for a MIMO system respectively

$G, G = \{g_{ij}\}$ The compensator or controller for a MISO system and the mxm compensator or controller matrix for a MIMO system, respectively. For a diagonal matrix $G = \{g_{ij}\}$

γ, γ_i The phase margin angle for the MISO system and for the i^{th} loop of the MIMO system, respectively

J The number of plant transfer functions for a MISO system or plant matrix for a MIMO system that describes the region of plant parameter uncertainty where $i = 1, 2, \dots, J$ denotes the particular plant case in the region of plant parameter uncertainty

λ The excess of poles over zeros of a transfer function

L_o, L_{o_i} The optimal loop transmission function for the MISO system and the i^{th} loop of the MIMO system, respectively

M_L, M_{L_i} The specified closed-loop frequency domain overshoots constraint for the MISO system and for the i^{th} loop of a MIMO system, respectively. This overshoot constraint may be dictated by the phase margin angle for the specified loop transmission function

$\Im P(j\omega_i)$ Script cap tee in conjunction with P denotes a template, i.e., $\Im P(j\omega_i)$ and $\Im Q(j\omega_i)$ frequency, for a MISO and MIMO plants respectively

T_{rU} The desired MISO tracking control ratio that satisfies the specified upper bound FOM

T_{nl} The desired MISO tracking control ratio that satisfies the specified lower bound FOM

T_d The desired MISO disturbance control ratio which satisfies the specified FOM

UAV Unmanned Aerial Vehicle

BNIA Basically Non-interacting

8. Acknowledgement

The work of this chapter is supported by Natural Science Basic Research Plan in Shaanxi Province of China (Program No. 2011GQ8005) and Northwestern Polytechnical University Foundation for Fundamental Research (No. :NPU-FFR-JC20100216)

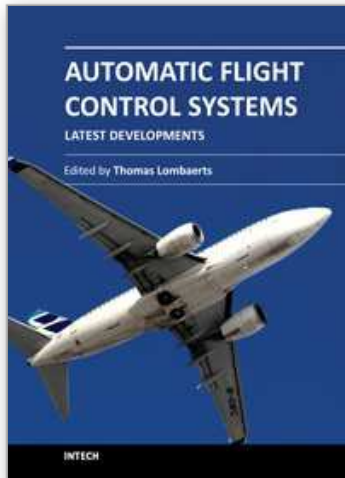
9. References

- Chen Huaimin: An Integrated QFT/EA Controller Design Method for a UAV's Lateral Flight Control System, *Mechanical Science and Technology*, Vol.27-3(2008),p. 413.
- Constantine H. Houpis, Steven J. Rasmussen. *Quantitative Feedback Theory: Fundamentals and Applications*[M], Marcel Dekker, Inc. New York, Basel
- Horowitz I. M, and M. Sidi, "Synthesis of Feedback Systems with Large Plant Ignorance for Prescribed Time Domain Tolerances," *Int. J. of Control*, vol. 16, pp 287-309, 1973.
- Horowitz, I. M. and C. Loecher, "Design 3x3 Multivariable Feedback System with Large Plant Uncertainty," *Int. J. Control*, vol. 33, pp. 677-699, 1981.
- Ibid, "Synthesis of Feedback Systems with Non-Linear Time Uncertain Plants to Satisfy Quantitative Performance Specifications ," *IEEE Proc.*, vol. 64, pp. 123-130, 1976.
- Houpis, C. H. "Quantitative Feedback Theory (QFT) for the Engineer: A Paradigm for the Design of Control Systems for Uncertain Systems," WL-TR-95-3061, AF Wright Laboratory, Wright-Patterson AFB, OH, 1995 (Available from National Technical Information Service, 5285 Port Royal Road, Springfield, VA 22151, document number AD-A297571.)
- Houpis, C. H. and P. R. Chandler, Editors: "Quantitative Feedback Theory Symposium Proceedings," WL-TR-92-3063, Wright Laboratories, Wright-Patterson AFB, OH, 1992.
- O Yaniv, Y Chait: A Simplified Multi-Input Multi-Output Formulation for Quantitative Feedback Theory, *Journal of Dynamic Systems, Measurement, and Control*, Vol.114-6(1998),p.179.
- Reynolds, O. R., M Pachter, and C. H. Houpis. "Design of a Subsonic Flight Control System for the Vista F-16 Using Quantitative Feedback Theory," *Proceedings of the American Control Conference*, pp. 350-354, 1994.
- Thompson, D. F., and O. D. I. Nwokah, "Optimal Loop Synthesis in Quantitative Feedback Theory," *Proceedings, of the American Control Conference*, San Diego, CA, pp.626-631, 1990.

Trosen, D. W., M, Pachter, and C. H. Houpis, "Formation Flight Control Automation," Proceedings of the American Institute of Aeronautics and Astronautics (AIAA) Conference, pp. 1379-1404, Scottsdale, AZ, 1994.

IntechOpen

IntechOpen



Automatic Flight Control Systems - Latest Developments

Edited by Dr. Thomas Lombaerts

ISBN 978-953-307-816-8

Hard cover, 204 pages

Publisher InTech

Published online 18, January, 2012

Published in print edition January, 2012

The history of flight control is inseparably linked to the history of aviation itself. Since the early days, the concept of automatic flight control systems has evolved from mechanical control systems to highly advanced automatic fly-by-wire flight control systems which can be found nowadays in military jets and civil airliners. Even today, many research efforts are made for the further development of these flight control systems in various aspects. Recent new developments in this field focus on a wealth of different aspects. This book focuses on a selection of key research areas, such as inertial navigation, control of unmanned aircraft and helicopters, trajectory control of an unmanned space re-entry vehicle, aeroservoelastic control, adaptive flight control, and fault tolerant flight control. This book consists of two major sections. The first section focuses on a literature review and some recent theoretical developments in flight control systems. The second section discusses some concepts of adaptive and fault-tolerant flight control systems. Each technique discussed in this book is illustrated by a relevant example.

How to reference

In order to correctly reference this scholarly work, feel free to copy and paste the following:

Xiaojun Xing and Dongli Yuan (2012). Quantitative Feedback Theory and Its Application in UAV's Flight Control, Automatic Flight Control Systems - Latest Developments, Dr. Thomas Lombaerts (Ed.), ISBN: 978-953-307-816-8, InTech, Available from: <http://www.intechopen.com/books/automatic-flight-control-systems-latest-developments/quantitative-feedback-theory-and-its-application-in-uav-s-flight-control>

INTECH
open science | open minds

InTech Europe

University Campus STeP Ri
Slavka Krautzeka 83/A
51000 Rijeka, Croatia
Phone: +385 (51) 770 447
Fax: +385 (51) 686 166
www.intechopen.com

InTech China

Unit 405, Office Block, Hotel Equatorial Shanghai
No.65, Yan An Road (West), Shanghai, 200040, China
中国上海市延安西路65号上海国际贵都大饭店办公楼405单元
Phone: +86-21-62489820
Fax: +86-21-62489821

© 2012 The Author(s). Licensee IntechOpen. This is an open access article distributed under the terms of the [Creative Commons Attribution 3.0 License](#), which permits unrestricted use, distribution, and reproduction in any medium, provided the original work is properly cited.

IntechOpen

IntechOpen